Direct Imaging of Exoplanets

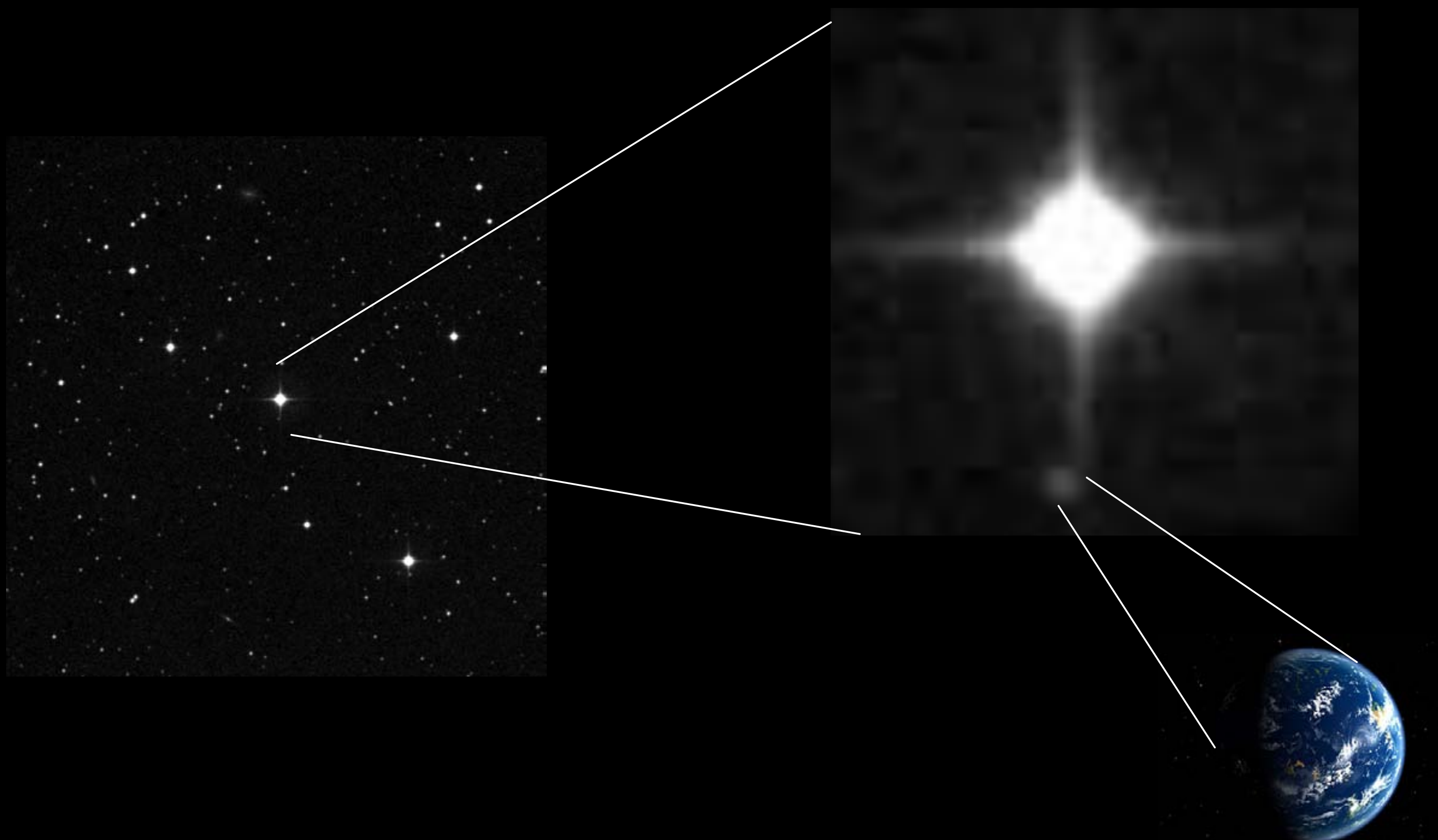

Techniques & Results

Challenge 1: Large ratio between star and planet flux (Star/Planet)

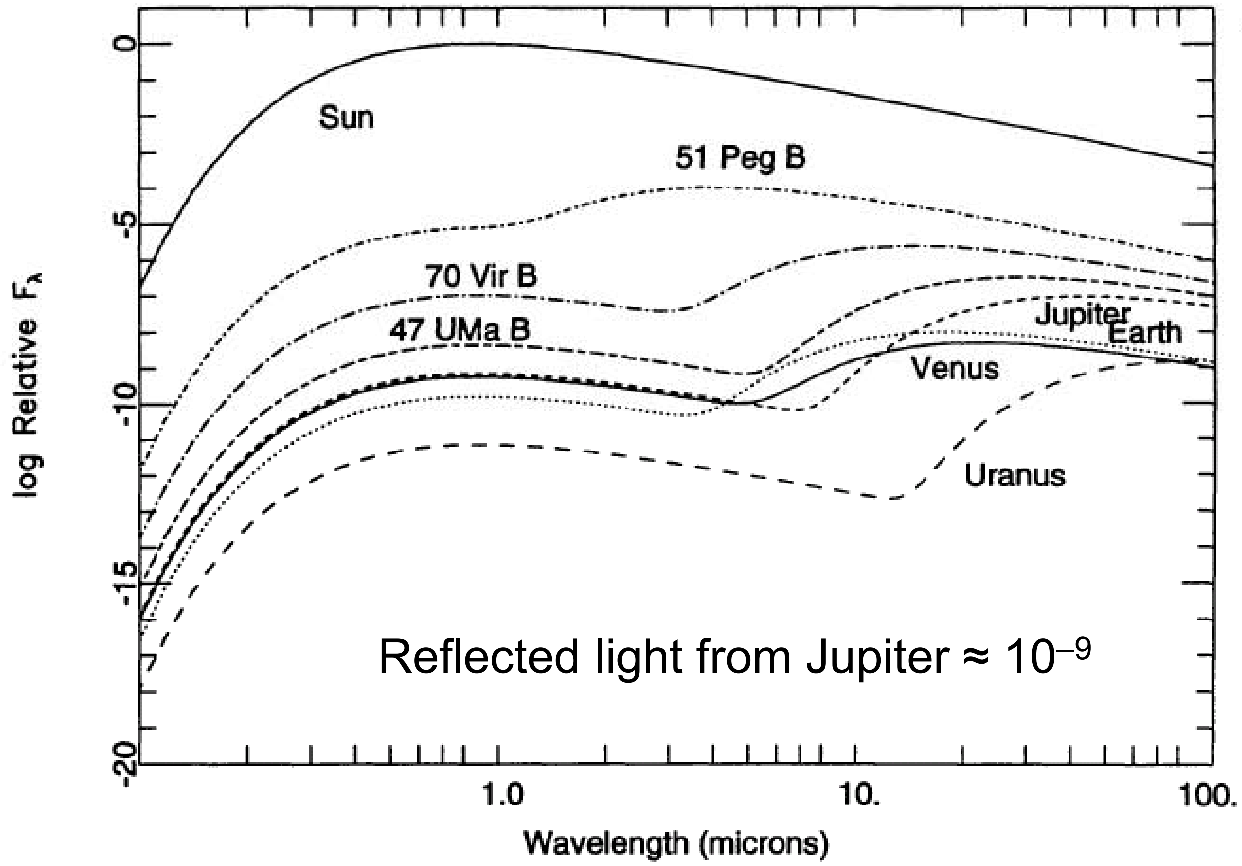

Figure 1. Relative fluxes of the Sun, Venus, Earth, Jupiter, Uranus, and the companion objects to 51 Pegasi, 70 Virginis, and 47 Ursae Majoris from 0.10 μm to 100 μm.


Stars are a billion times brighter…


...than the planet
...hidden
in the glare.

Challenge 2: Close proximity of planet to host star

Planet	Mass (M_{Jup})	Semi-axis (AU)	Dist (pcs)	Sep (mas)	Sp. Type
Eps Eri b	1.55	3.39	3.2	1060	K2 V
GJ 674 b	0.037	0.039	4.54	8.6	M2.5
Gliese 876 b	1.935	0.20783	4.72	43.8	M4 V
Gliese 876 c	0.56	0.13		27.5	
Gliese 876 d	0.018	0.0208067		4.2	
GJ 832 b	0.64	3.4	4.94	688	
Gl 581 b	0.0492	0.041	6.26	6.5	M3
Gl 581 c	0.0158	0.073		11.7	
Gl 581 d	0.0243	0.25		39.9	
GJ 849 b	0.82	2.35	8.8	267.0	M3.5
GJ 317 b	1.2	0.95	9.17	103.6	M3.5
HD 285968 b	0.0265	0.066	9.4	7.02	M2.5V
GJ 436 b	0.072	0.02872	10.2	2.81	M2.5
HD 62509 b	2.9	1.69	10.34	163.4	K0IIIb
Gl 86 b	4.01	0.11	11	10.0	K1V
HD 3651 b	0.2	0.284	11	25.8	K0 V
HD 69830 b	0.033	0.0785	12.6	6.23	K0V
HD 69830 c	0.038	0.186	12.6	14.8	
HD 69830 d	0.058	0.63	12.6	49.2	
HD 40307 b	0.0132	0.047	12.8	3.7	K2.5V
HD 40307 c	0.0216	0.081	12.8	6.3	V
HD 40307 d	0.0288	0.134	12.8	10.5	V
HD 147513 b	1.0	1.26	12.9	97.7	G3/G5V
55 Cnc b	0.824	0.115	13.02	8.8	G8 V
55 Cnc c	0.169	0.24	13.02	18.4	
55 Cnc d	3.835	5.77	13.02	443.1	
55 Cnc e	0.034	0.038	13.02	2.91	
55 Cnc f	0.144	0.781	13.02	60.0	
Ups And b	0.69	0.059	13.47	4.4	F8 V
Ups And c	1.98	0.83	13.47	61.6	
Ups And d	3.95	2.51	13.47	186.3	
γ Cep b	1.6	2.044	13.79	148.22	K2 V
47 Uma b	2.6	2.11	13.97	151.0	G0V
47 Uma c	0.46	3.39	13.97	242.7	
51 Peg b	0.468	0.052	14.7	3.5	G2 IV
τ Boo b	3.9	0.046	15	3.1	F7 V
HD 160691 b	1.67	1.5	15.3	751.6	G3 IV-V
HD 160691 c	3.1	4.17	15.3	272.5	
HD 160691 d	0.044	0.09	15.3	5.9	
HD 160691 e	0.5219	0.921	15.3	33.5	
HR 810 b	1.94	0.91	15.5	58.7	G0V
HD 190360 c	0.057	0.128	15.89	8.0	G6 IV
HD 190360 b	1.502	3.92	15.89	246.7	

Direct Detections need contrast ratios of 10^{-9} to 10^{-10}

At separations of 0.01 to 1 arcseconds

Earth : $\sim 10^{-10}$ separation = 0.1 arcseconds for a star at 10 parsecs

Jupiter: $\sim 10^{-9}$ separation = 0.5 arcseconds for a star at 10 parsecs

1 AU = 1 arcsec separation at 1 parsec

Younger planets are hotter and they emit more radiated light. These are easier to detect.

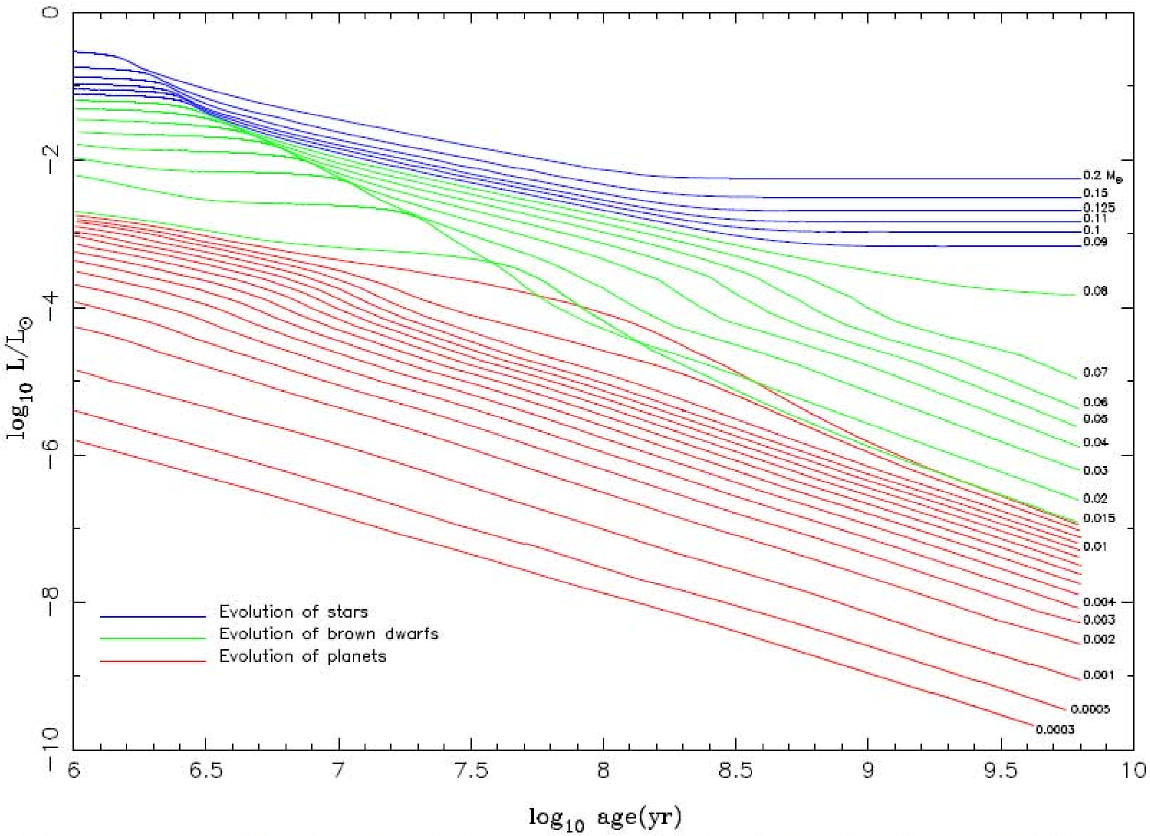

Figure 1. Evolution of the luminosity (in $L_\odot$) of solar–metallicity M dwarfs and substellar objects versus time (in years) after formation. The stars, "brown dwarfs" and "planets" are shown as solid, dashed, and dot–dashed curves, respectively. In this figure, we arbitrarily designate as "brown dwarfs" those objects that burn deuterium, while we designate those that do not as "planets." The masses in $M_\odot$ label most of the curves, with the lowest three corresponding to the mass of Saturn, half the mass of Jupiter, and the mass of Jupiter.

Adaptive Optics : An important component for any imaging instrument

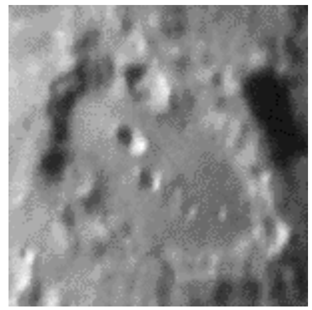

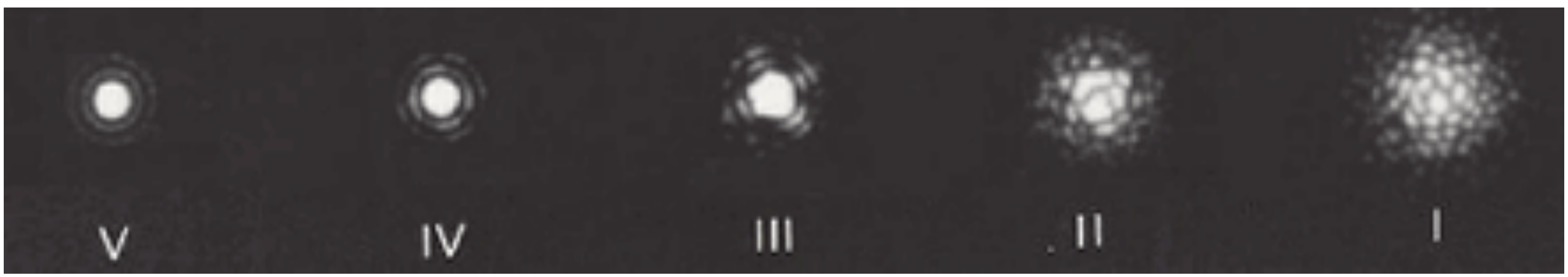

Atmospheric turbulence distorts stellar images making them much larger than point sources. This seeing image makes it impossible to detect nearby faint companions.

Adaptive Optics (AO)

The scientific and engineering discipline whereby the performance of an optical signal is improved by using information about the environment through which it passes

AO Deals with the control of light in a real time closed loop and is a subset of *active optics.*

Adaptive Optics: Systems operating below 1/10 Hz

Active Optics: Systems operating above 1/10 Hz

Example of an Adaptive Optics System: The Eye-Brain

The brain interprets an image, determines its correction, and applies the correction either voluntarily of involuntarily

Lens compression: Focus corrected mode

Tracking an Object: Tilt mode optics system

Iris opening and closing to intensity levels: Intensity control mode

Eyes squinting: An aperture stop, spatial filter, and phase controlling mechanism

The Ideal Telescope

$$P_0(\vec{\alpha}) = \frac{\pi D^2}{4\lambda^2}\left[\frac{2J_1(\pi D|\vec{\alpha}|/\lambda)}{\pi D|\vec{\alpha}|/\lambda)}\right]^2,$$

image of a star produced by ideal telescope

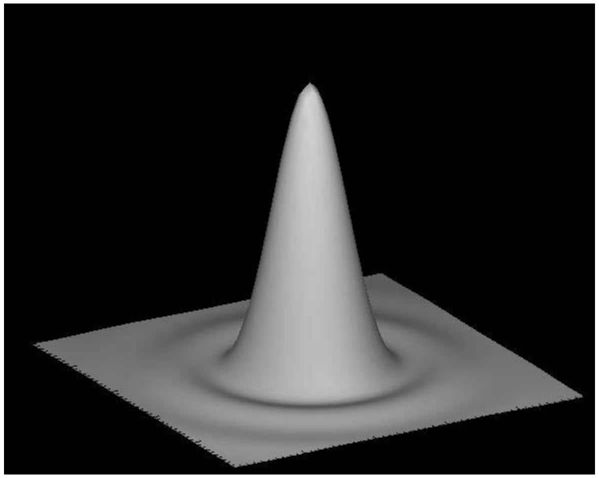

where:

- *P(α)* is the light intensity in the focal plane, as a function of angular coordinates α ;
- λ is the wavelength of light;
- D is the diameter of the telescope aperture;
- J_1 is the so-called Bessel function.

The first dark ring is at an angular distance D_λ of from the center.
This is often taken as a measure of resolution (diffraction limit) in an ideal telescope.

D_λ = 1.22 λ/D = 251643 λ/D (arcsecs)

Diffraction Limit

Telescope	5500 Å	2 μm	10 μm	Seeing
TLS 2m	0.06"	0.2"	1.0"	2"
VLT 8m	0.017"	0.06"	0.3"	0.2"
Keck 10m	0.014"	0.05"	0.25"	0.2"
ELT 42m	0.003"	0.01"	0.1"	0.2"

Even at the best sites AO is needed to improve image quality and reach the diffraction limit of the telescope. This is easier to do in the infrared

Atmospheric Turbulence

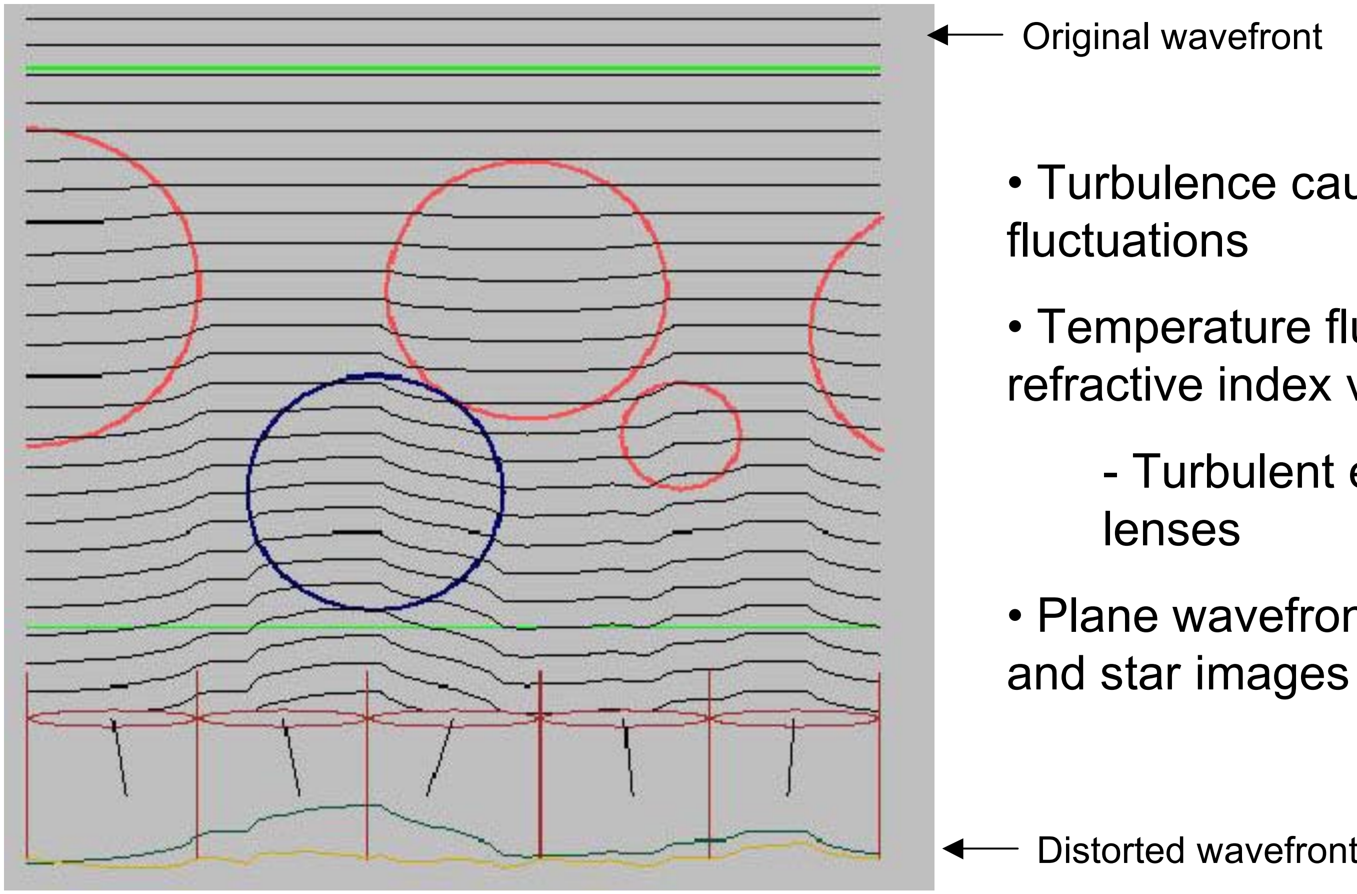

- Turbulence causes temperature fluctuations
- Temperature fluctuations cause refractive index variations
  - Turbulent eddies are like lenses
- Plane wavefronts are wrinkled and star images are blurred

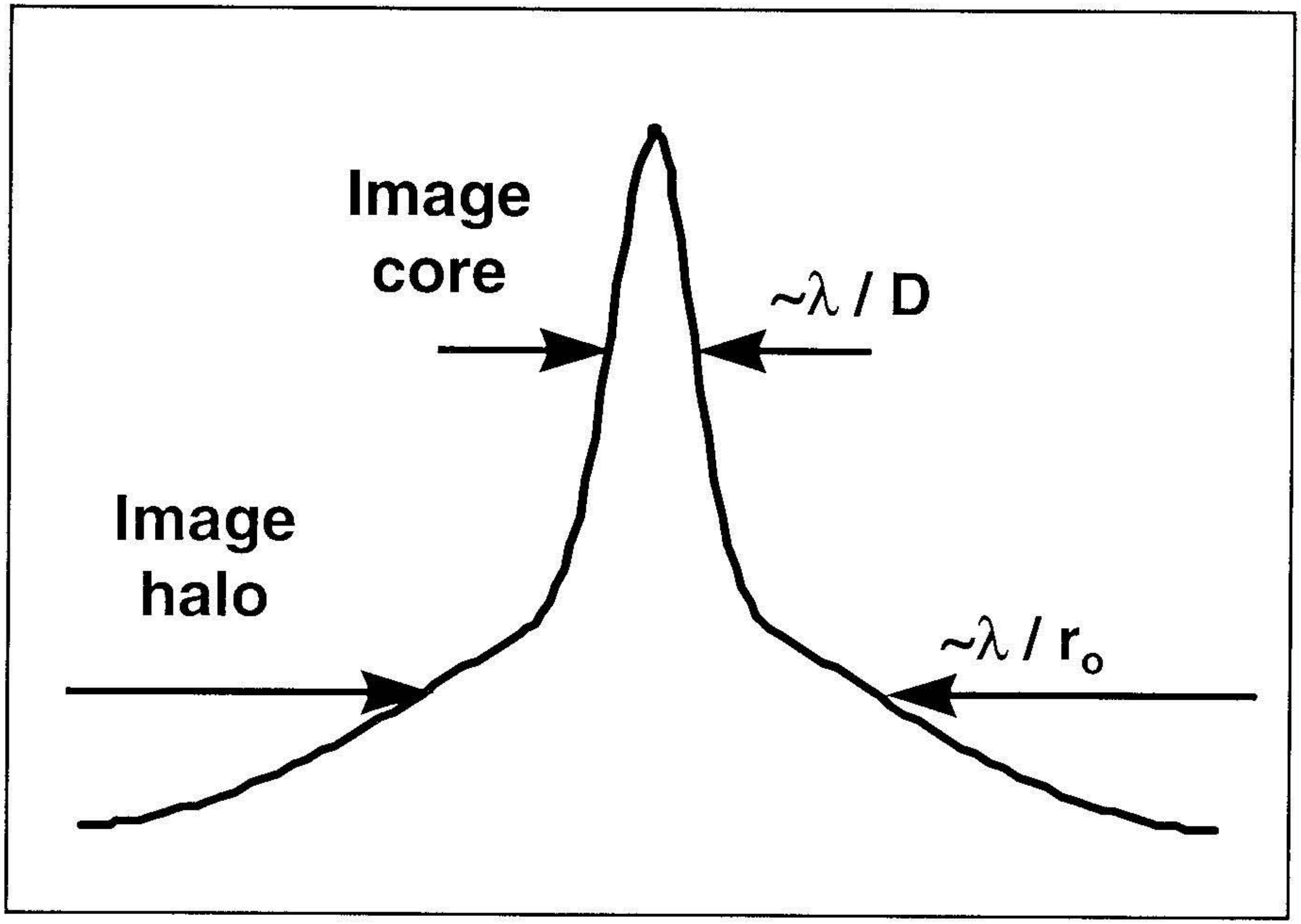

Figure 2.2: The point spread function through the atmosphere exhibits a diffraction-limited central core and a halo.

Basic Components for an AO System

1. You need to have a mathematical model representation of the wavefront
2. You need to **measure the incoming wavefront** with a point source (real or artifical).
3. You need to **correct the wavefront** using a deformable mirror

Shack-Hartmann Wavefront Sensor

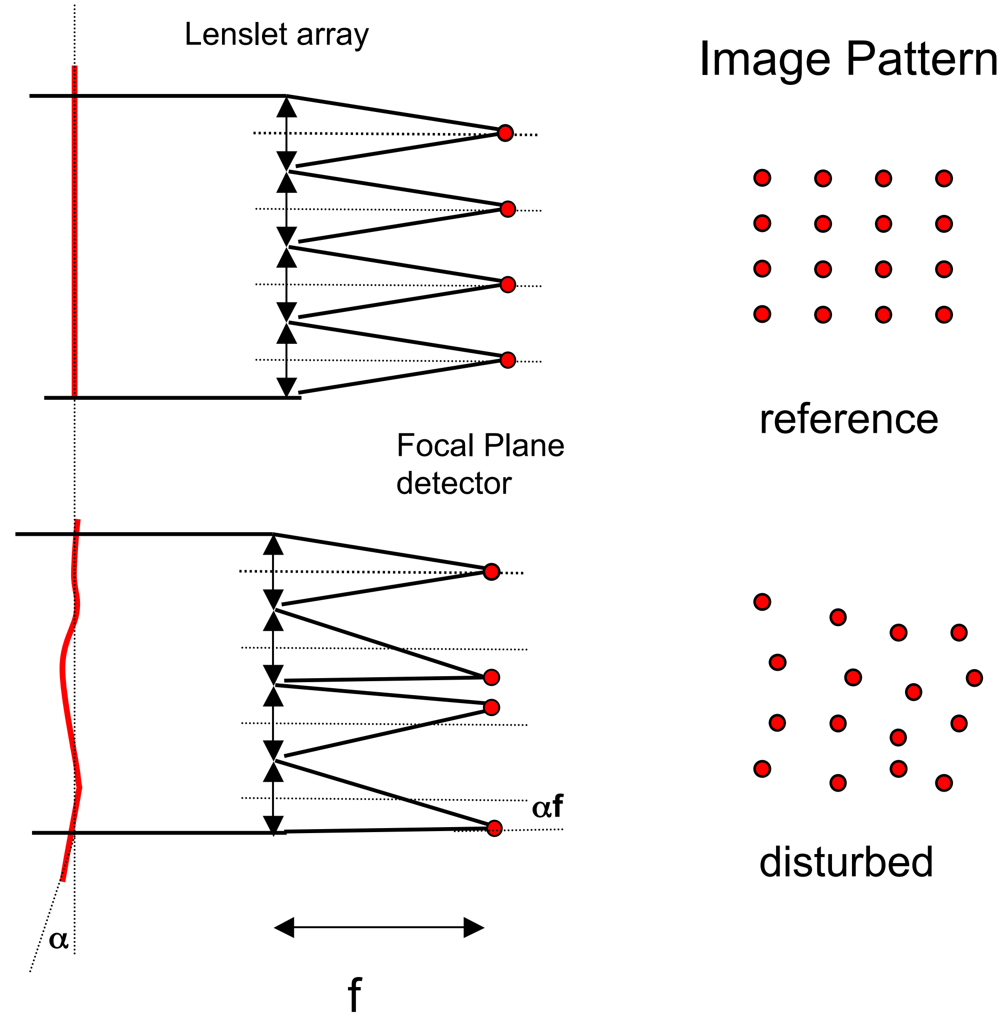

Shack-Hartmann Wavefront Sensor

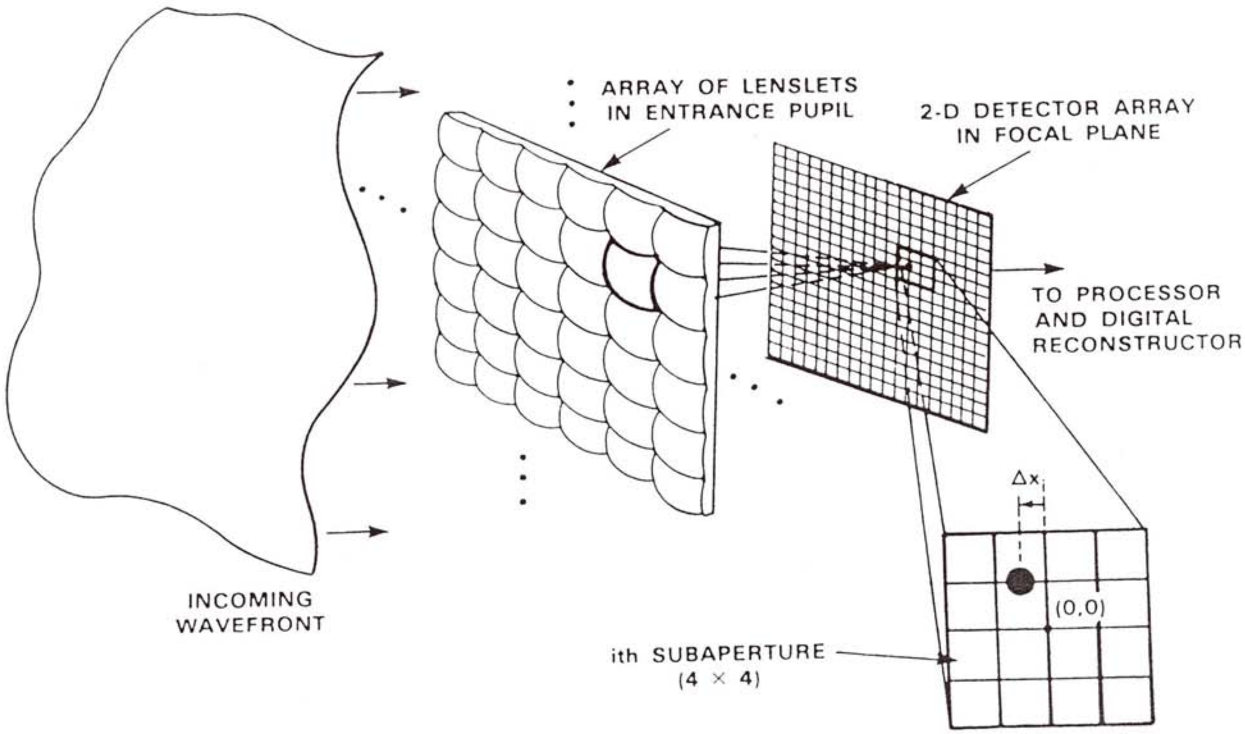

Figure 3 Principle of Hartmann-Shack wavefront sensor. The lenslets array produces an array of star images on the 2-dimensional detector array (generally a CCD or Intensified CCD). Tilt variations in the incoming, distorted wavefront result in position variations (Δx, Δy) of the star images on the detector. These are measured and fed to a digital processor which reconstructs the wavefront distortions. (From Murphy 1992; reprinted with permission of Lincoln Laboratory, MIT, Lexington, MA.)

Deformable mirrors

Deformable mirror from the Keck system

Rear View

349 Actuators
on 7 mm spacing

Front View

146 mm diameter
clear aperture

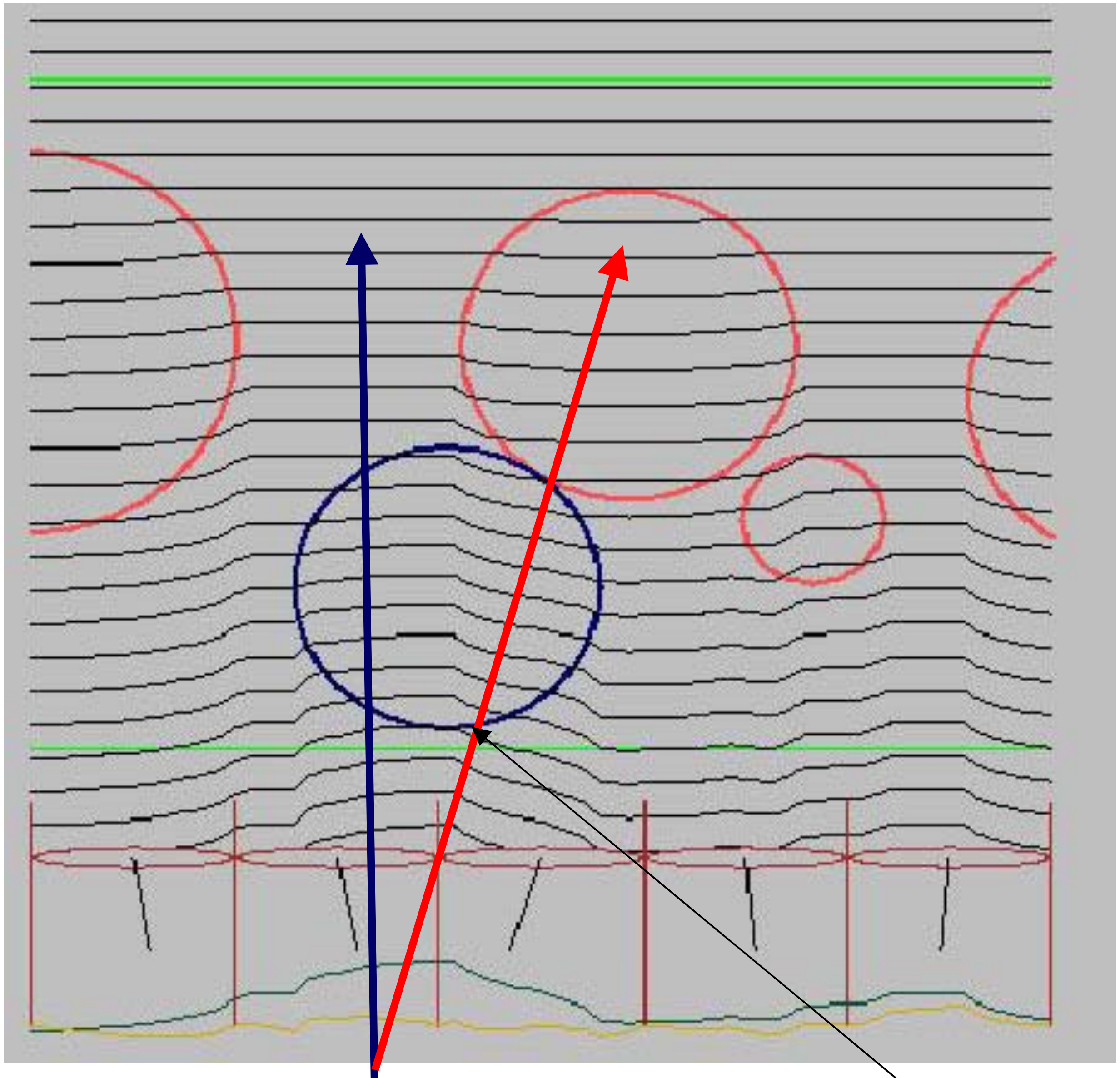

If you are observing an object here

You do not want to correct using a reference star in this direction

Reference Stars

You need a reference point source (star) for the wavefront measurement. The reference star must be within the isoplanatic angle, of about 10-30 arcseconds

If there is no bright (mag ~ 14-15) nearby star then you must use an artificial star or „laser guide star“.

All laser guide AO systems use a sodium laser tuned to Na 5890 Å pointed to the 11.5 km thick layer of enhanced sodium at an altitude of 90 km.

Much of this research was done by the U.S. Air Force and was declassified in the early 1990s.


© Laurie Hatch

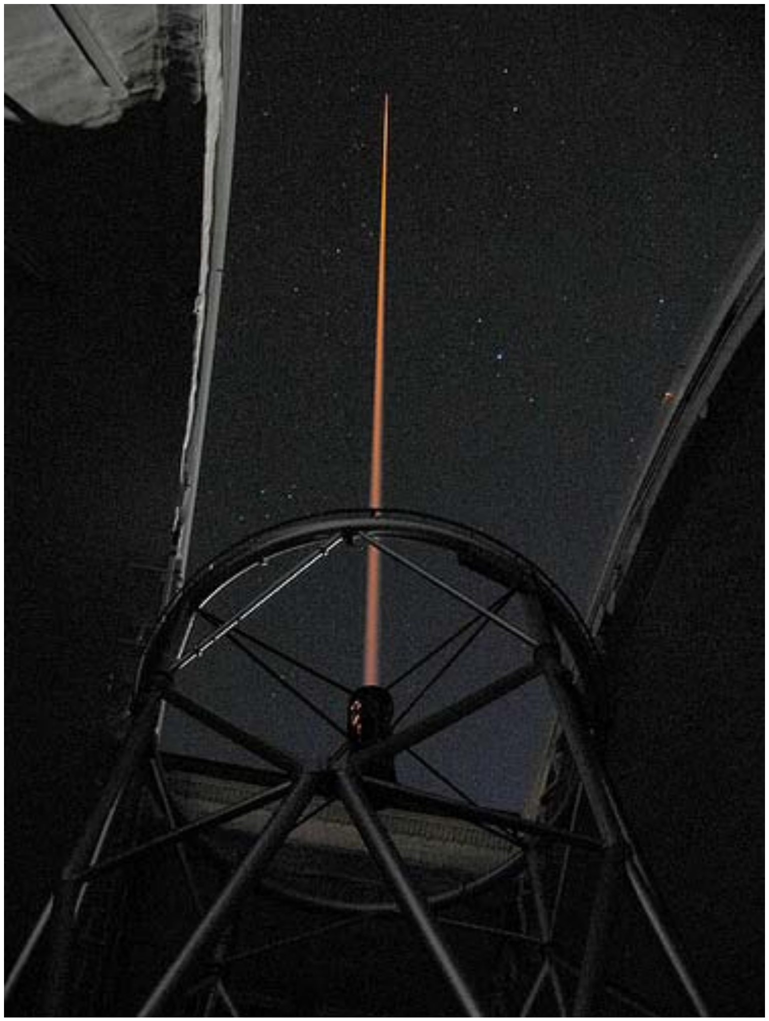

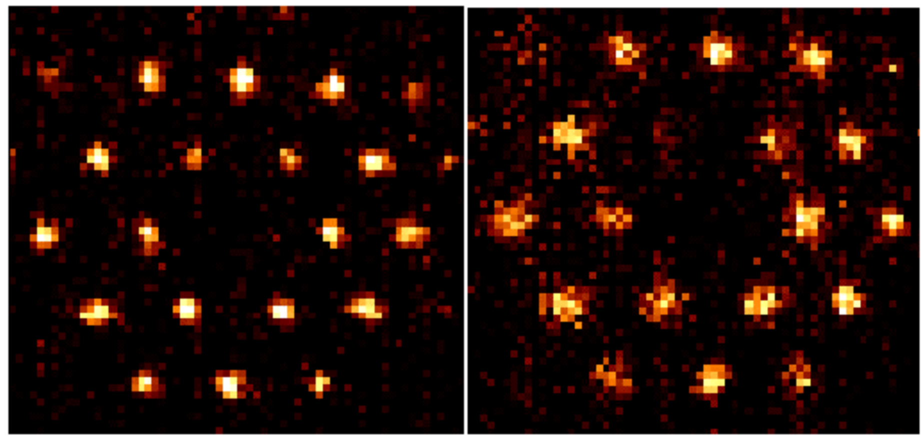

Images of a natural guide star (left) and the laser guide star (right) on the Shack-Hartmann sensor through the 5×5 lenslet array, and with a sampling rate of 100 Hz giving a disturbance rejection bandwidth of $\sim$10 Hz.

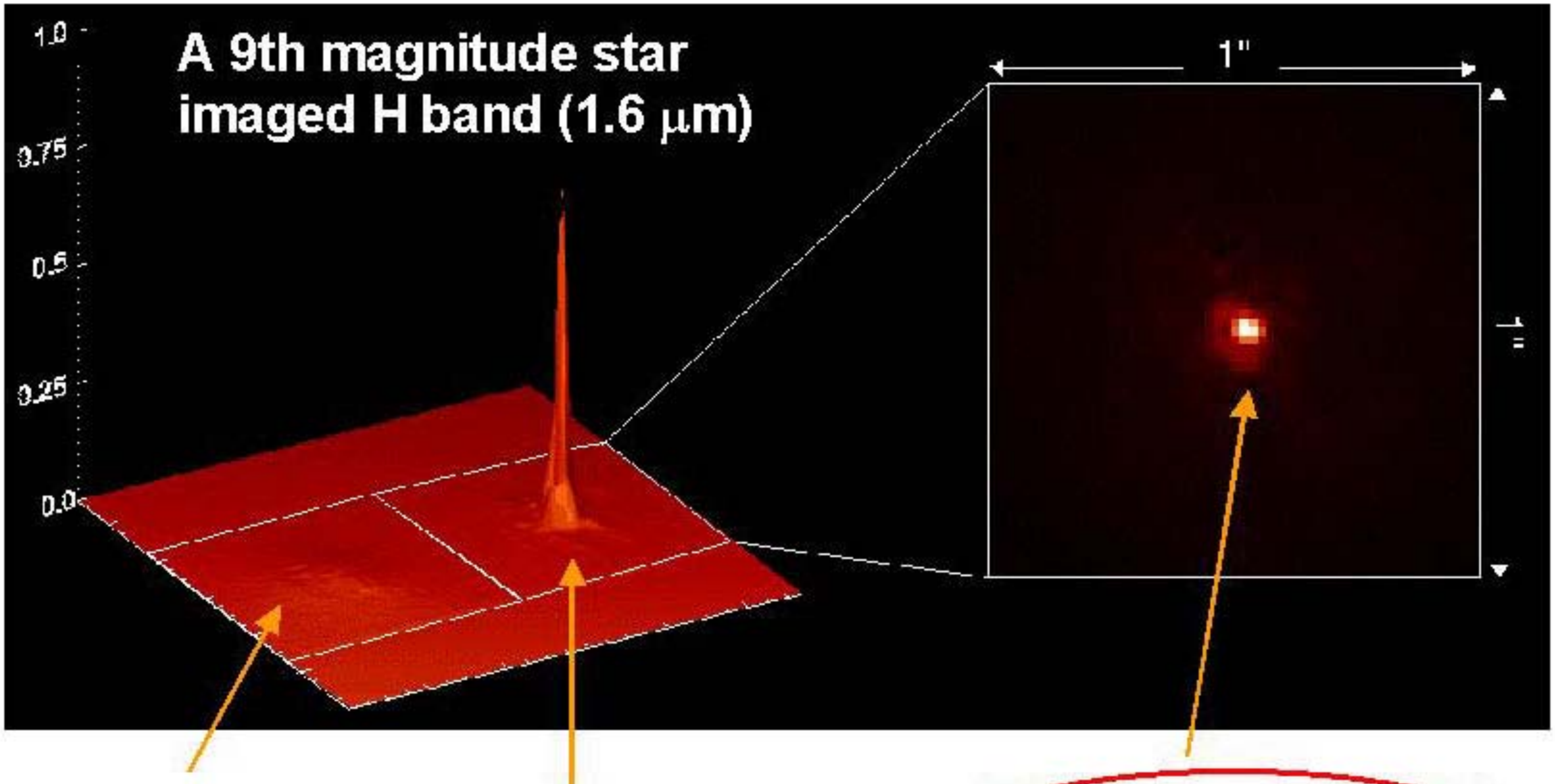

Without AO
FWHM 0.34 arc sec
Strehl = 0.6%

With AO

FWHM 0.04 arc sec
Strehl = 34%

Starfire Optical Range

Binary Star Image

3.5-m telescope with adaptive optics

First light for the adaptive optics system on the 3.5-m telescope at the Starfire Optical Range occurred in September, 1997. This astronomical I Band compensated image of the binary star k-Peg was generated using the 756 active actuator adaptive optics system.

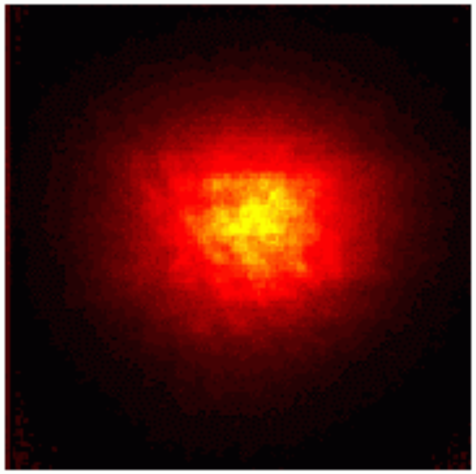

Uncompensated Image

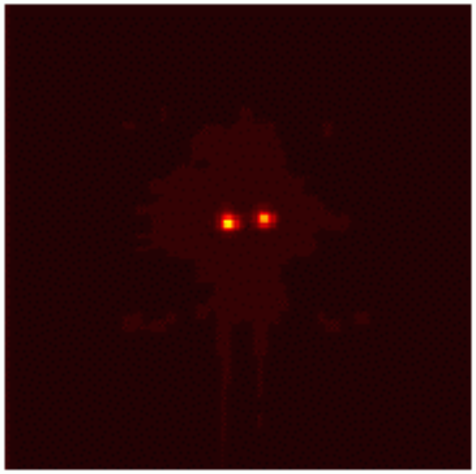

Compensated Image. 0.3 arcsec separation

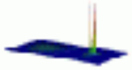 Open 65k jpeg	3 D plot of the binary star image.

Applications of Adaptive Optics

Sun, planets, stellar envelopes and dusty disks, young stellar objects, galaxies, etc. Can get 1/20 arcsecond resolution in the K band, 1/100 in the visible (eventually)

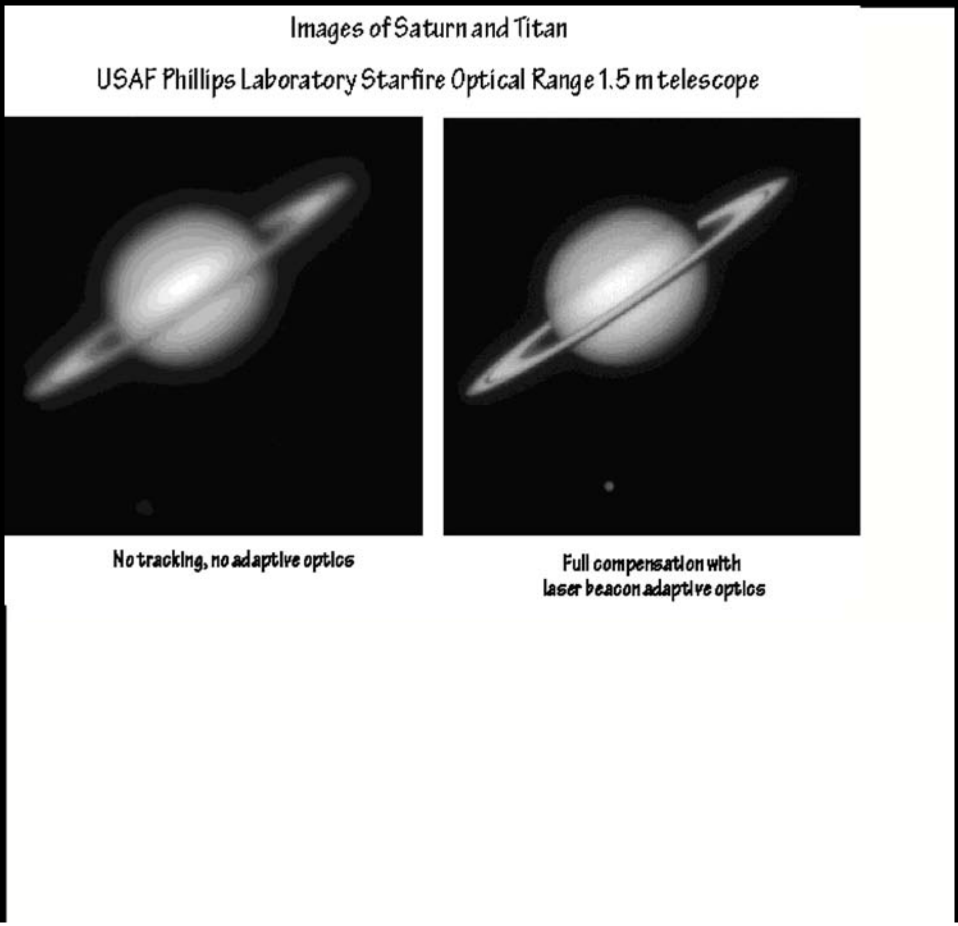

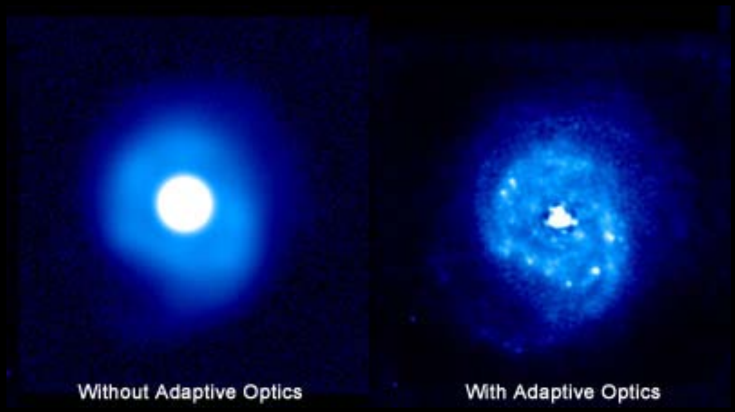

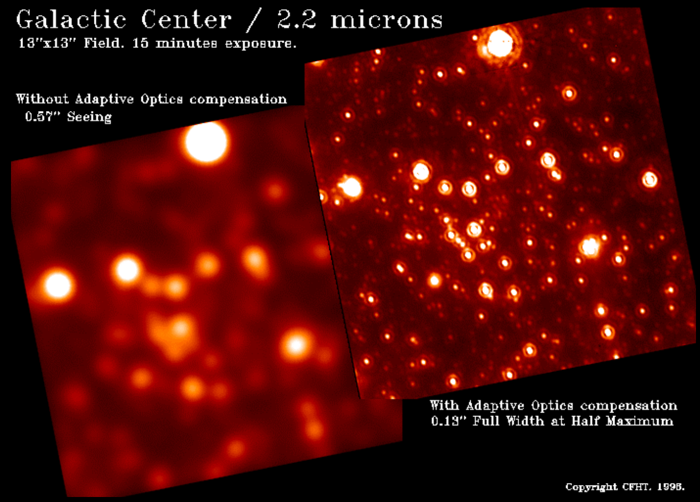

Applications of Adaptive Optics

Faint companions

The seeing disk will normally destroy the image of faint companion. Is needed to detect substellar companions (e.g. GQ Lupi)

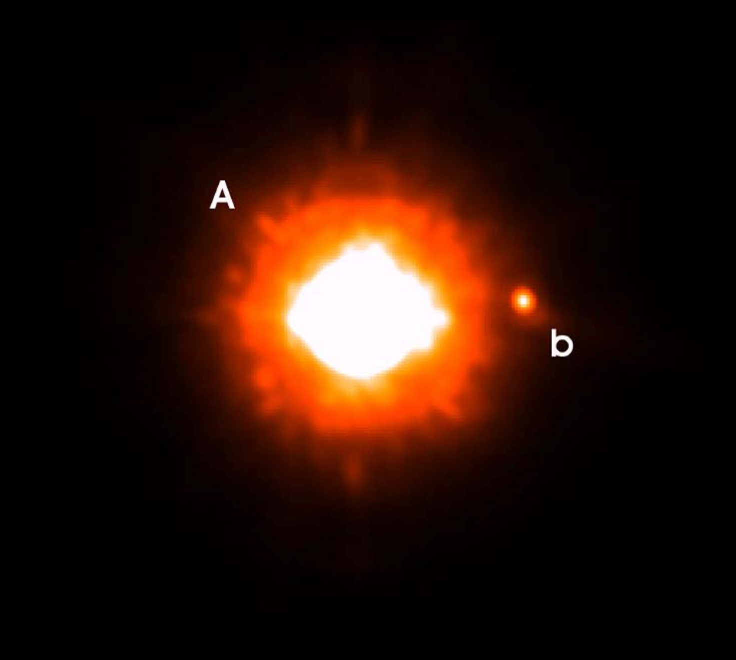

The Sub-Stellar Companion to GQ Lupi
(NACO/VLT)

ESO PR Photo 10a/05 (7 April 2005)

© European Southern Observatory

Applications of Adaptive Optics

Coronagraphy

With a smaller image you can better block the light. Needed for planet detection

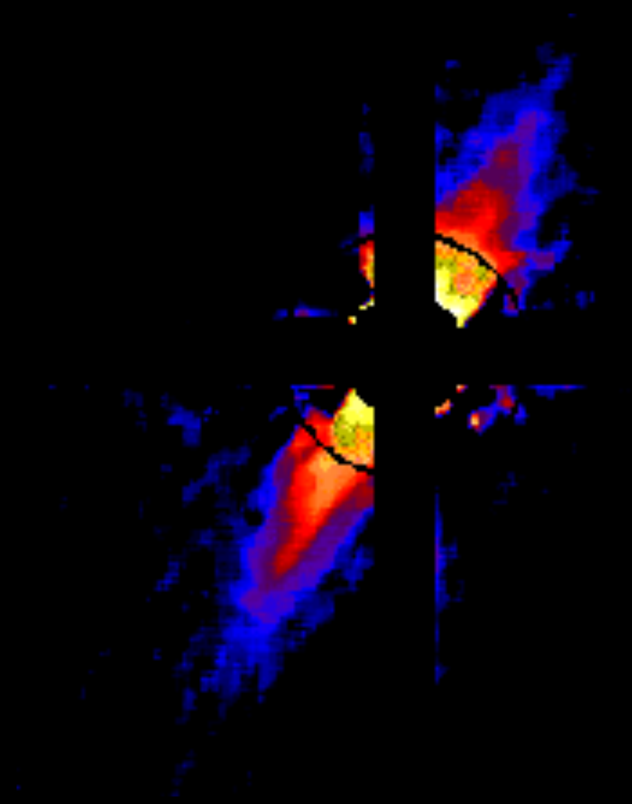

Coronagraphs

Bernard Lyot, 1939, at Pic du Midi
French Astronomer
Inventor of the Coronagraph

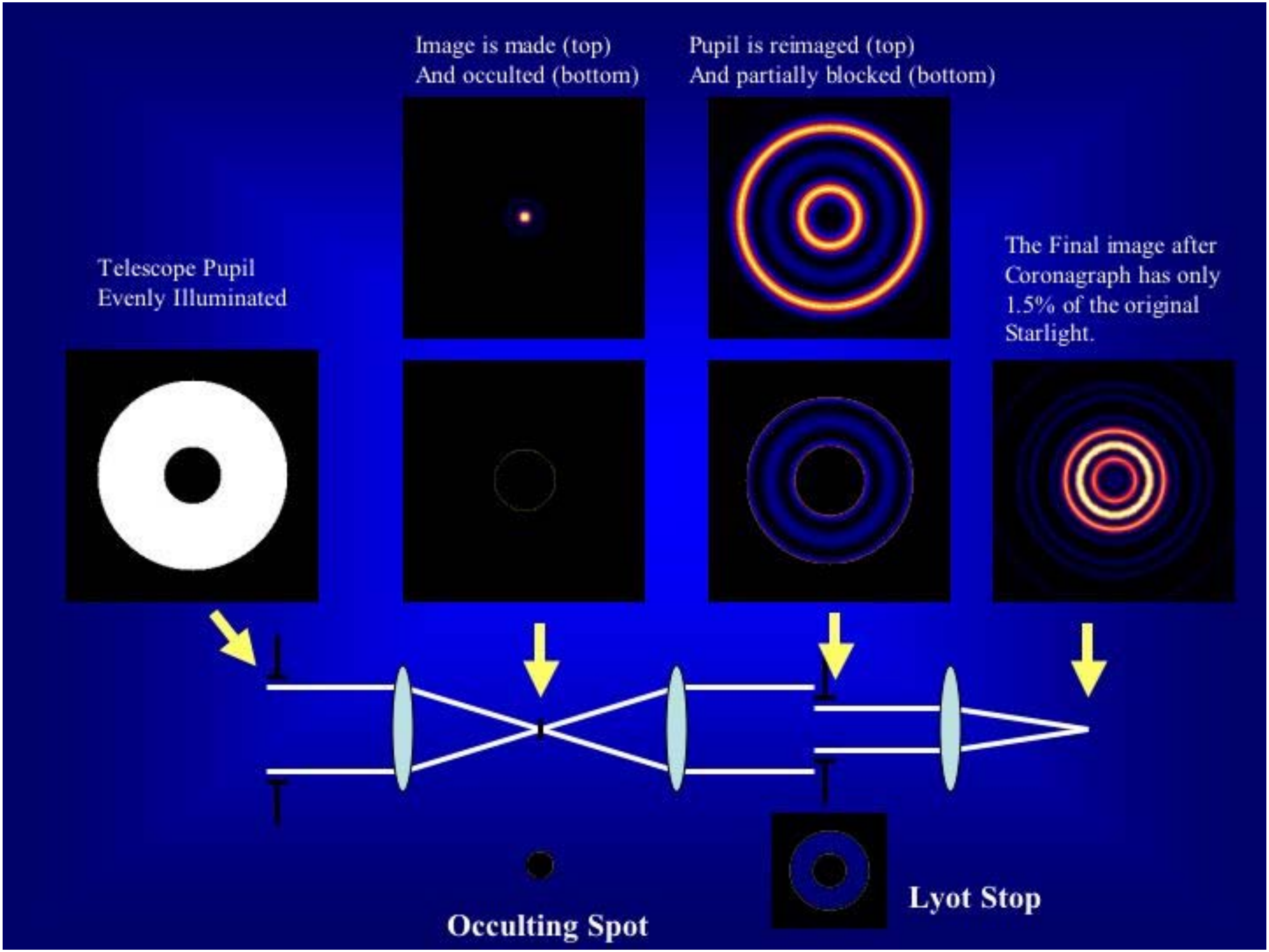
Image is made (top)
And occulted (bottom)
Pupil is reimaged (top)
And partially blocked (bottom)
Telescope Pupil
Evenly Illuminated
The Final image after
Coronagraph has only
1.5% of the original
Starlight.
Occulting Spot
Lyot Stop

Subtracting the Point Spread Function (PSF)

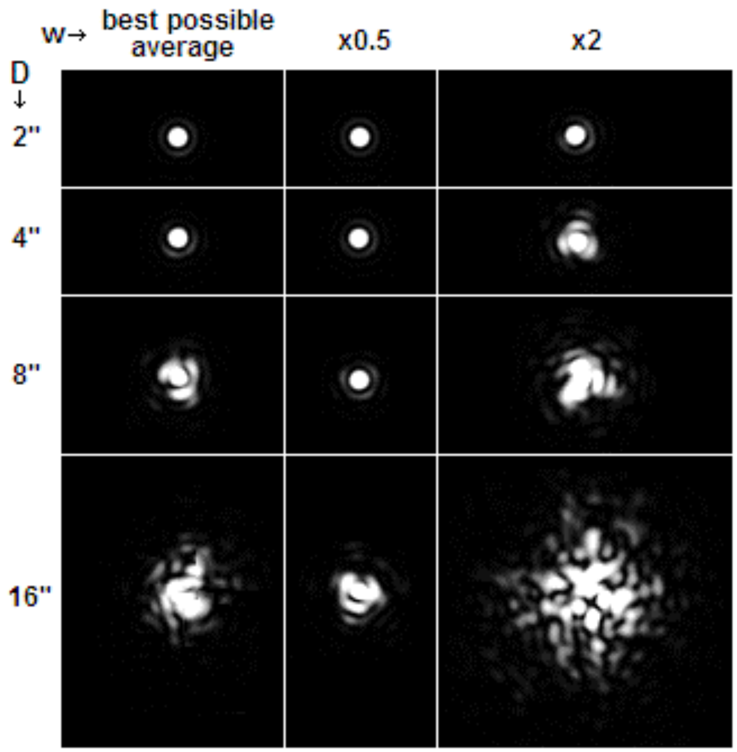

To detect close companions one has to subtract the PSF of the central star (even with coronagraphs) which is complicated by atmospheric speckles.

One solution: Differential Imaging

Nulling Interferometers

Adjusts the optical path length so that the wavefronts
from both telescope destructively interfere at the position of the star

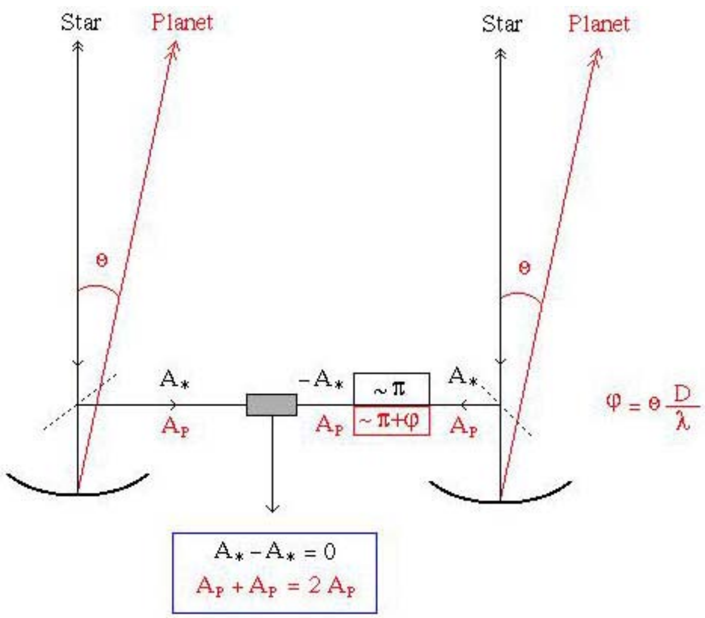

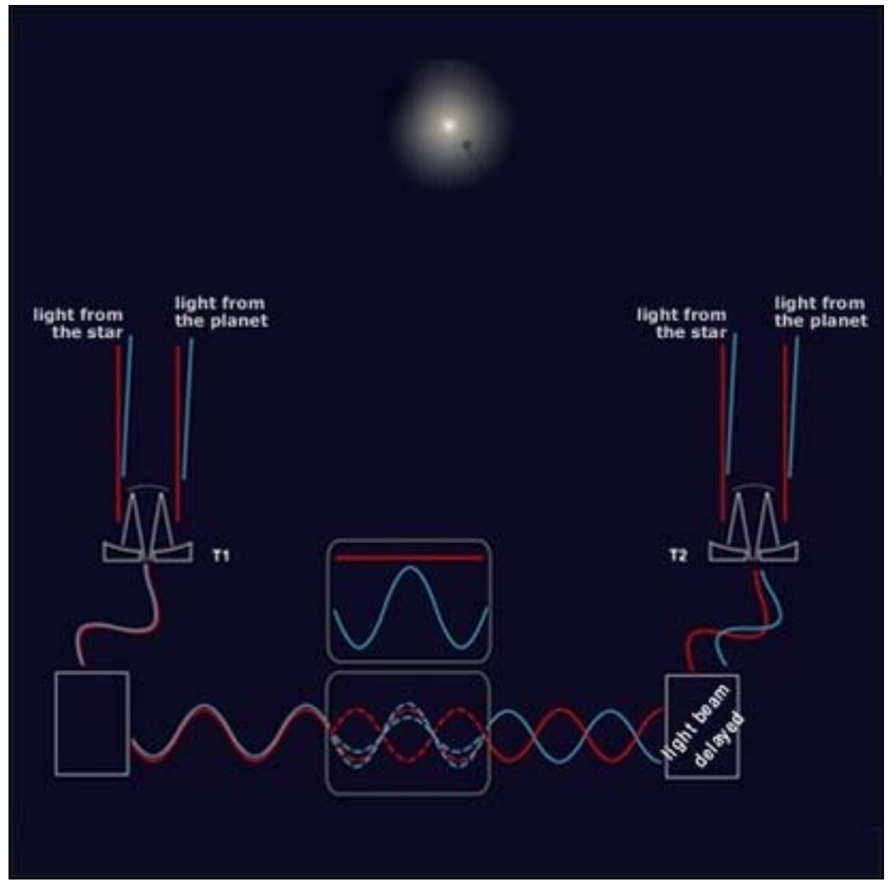

Technological challenges have
prevented nulling interferometry from
being a viable imaging method…for now

Darwin/Terrestrial Path Finder would have used Nulling Interferometry

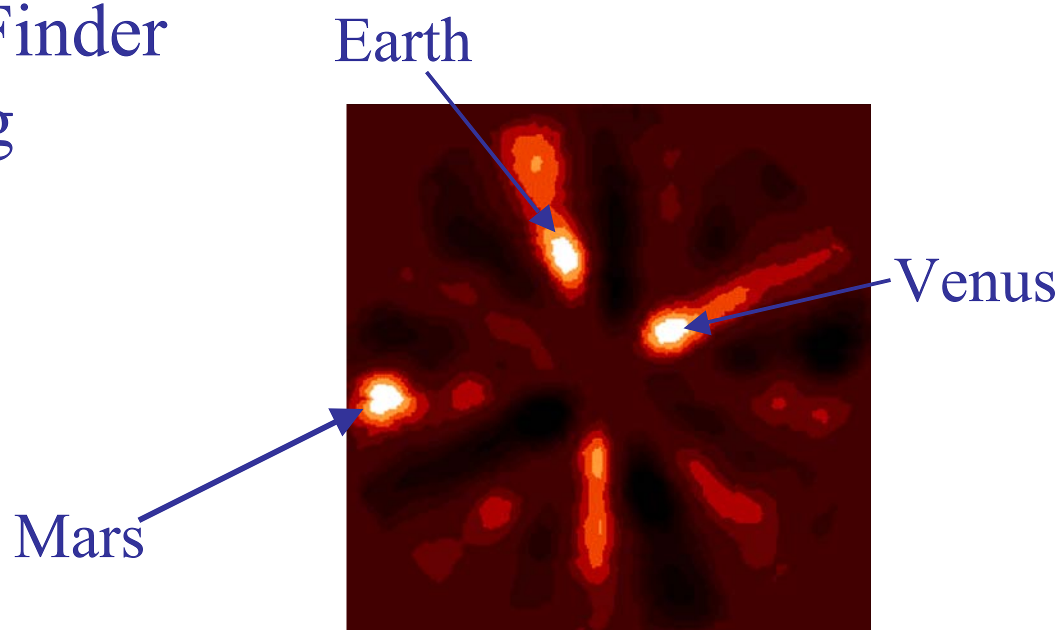

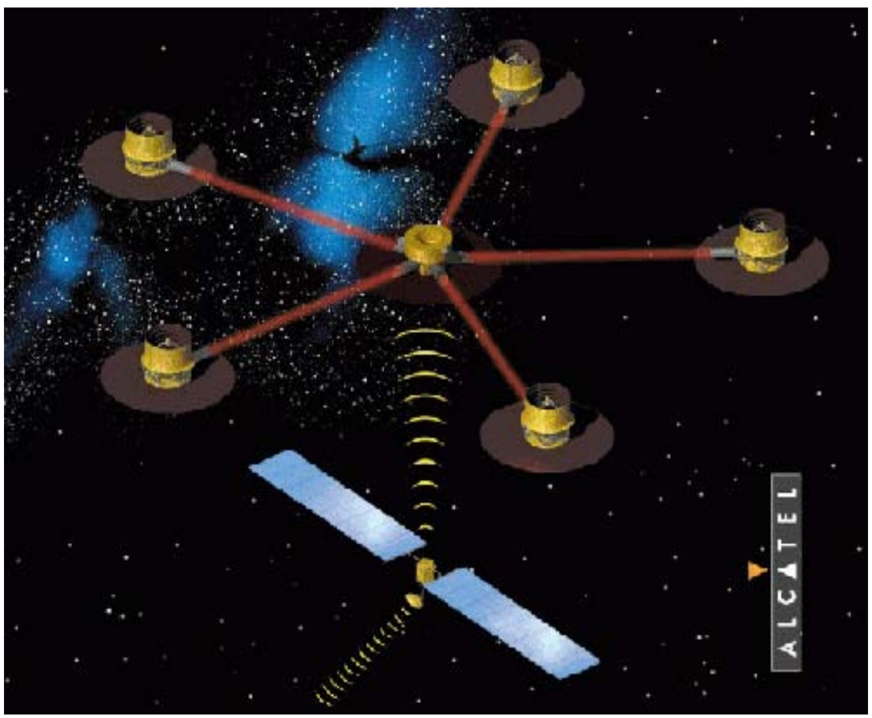

Ground-based European Nulling Interferometer Experiment will test nulling interferometry on the VLTI

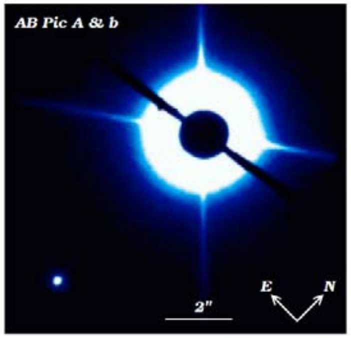

Fig. 1. K_s-band coronagraphic image of AB Pic A and b acquired on 17 March 2003 with an occulting mask of diameter 1.4″.

Results:
Pictures of Exoplanets!

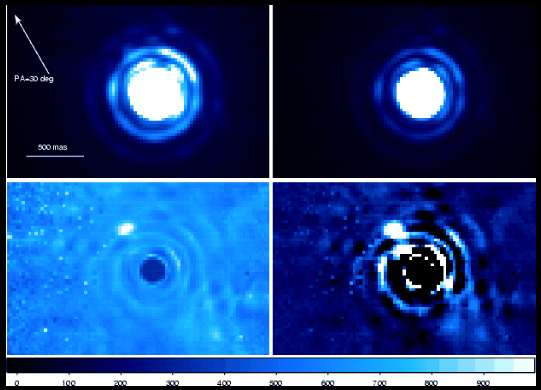

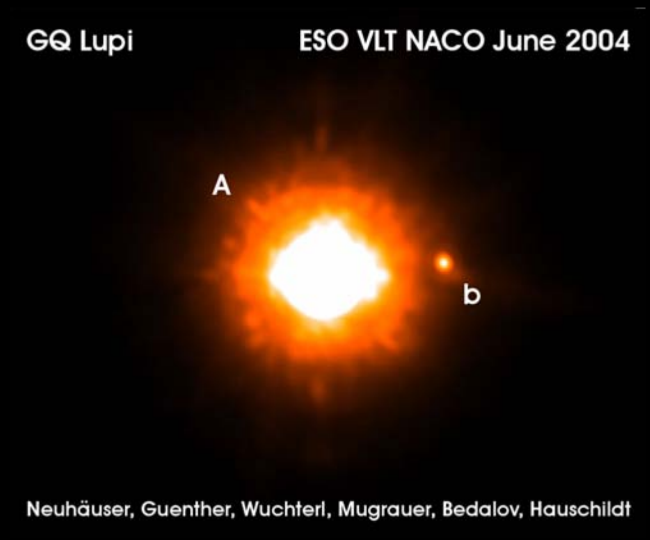

Coronography of Debris Disks

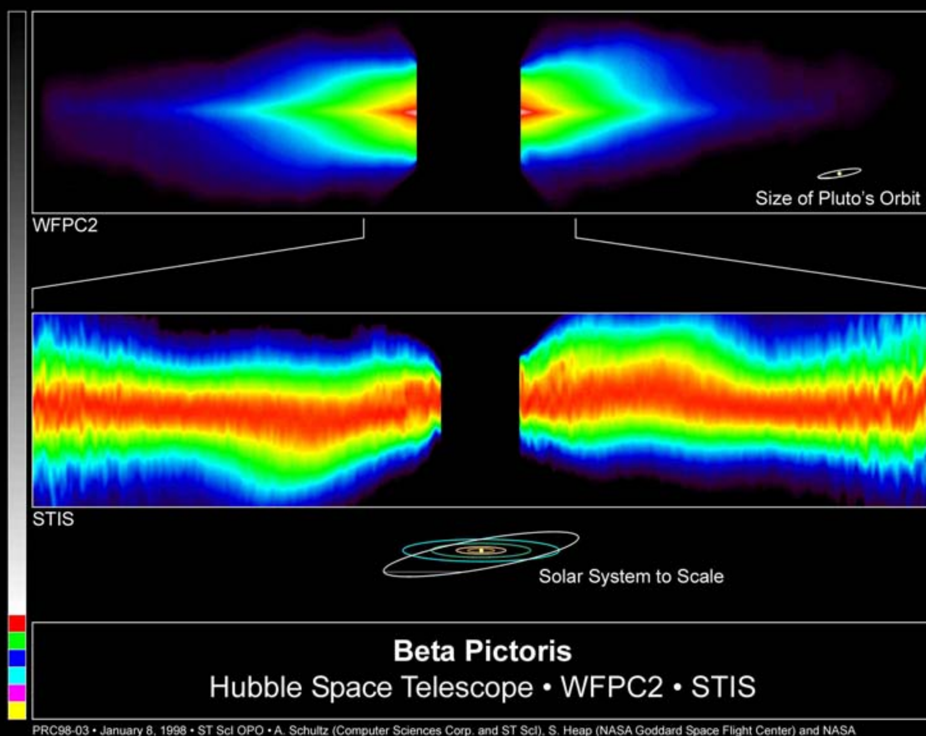

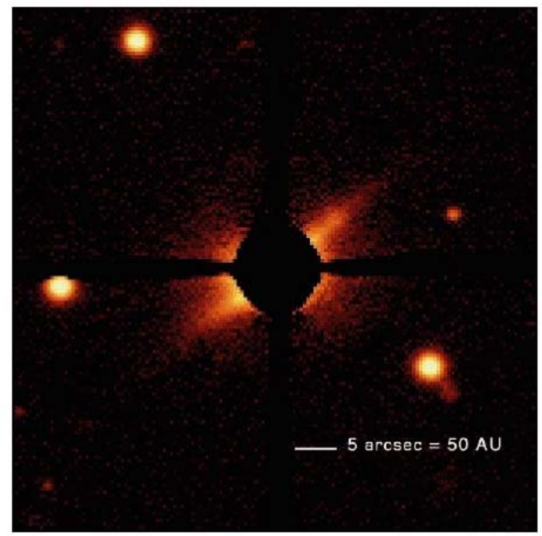

Fig. 1.— The disk surrounding AU Mic seen in optical scattered light. North is up, east is left, and each side of this false-color image corresponds to 60″. The central dark region is produced by the 9.5″ diameter focal plane occulting spot which is suspended by four wires and completely masks our direct view of the star. This image represents 900 seconds total integration in the R band and each pixel corresponds to 4 AU at the distance to AU Mic. Residual light evident near the occulting spot edge in the NE-SW direction is attributed to asymmetries in the point-spread function caused by instrumental scattering and atmospheric seeing.

Structure in the disks give hints to the presence of sub-stellar companions

Detection of a Brown Dwarf

Brown Dwarf Gliese 229B

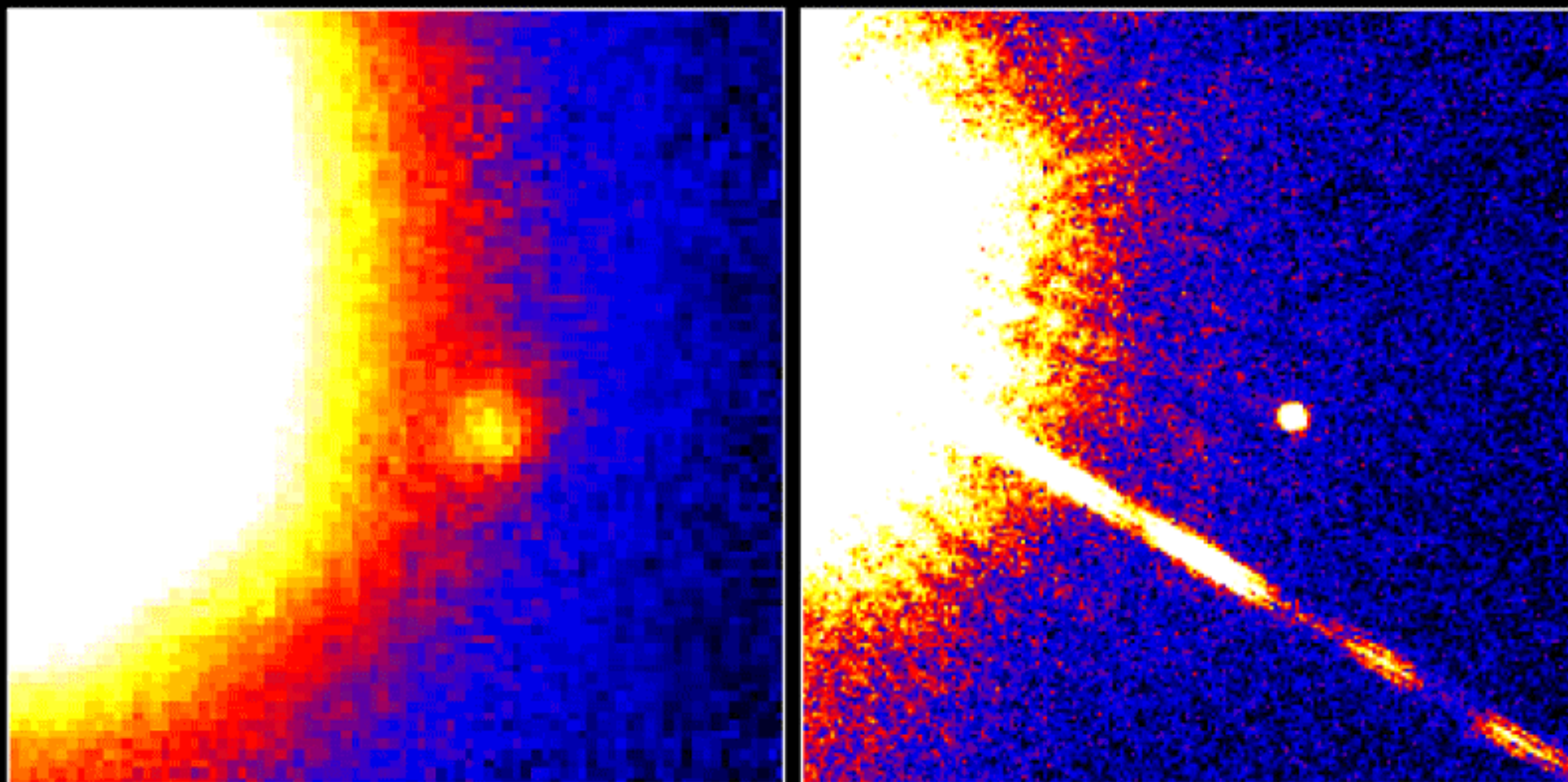

Palomar Observatory
Discovery Image
October 27, 1994

Hubble Space Telescope
Wide Field Planetary Camera 2
November 17, 1995

PRC95-48 • ST ScI OPO • November 29, 1995
T. Nakajima and S. Kulkarni (CalTech), S. Durrance and D. Golimowski (JHU), NASA

Spectral Features show Methane and Water

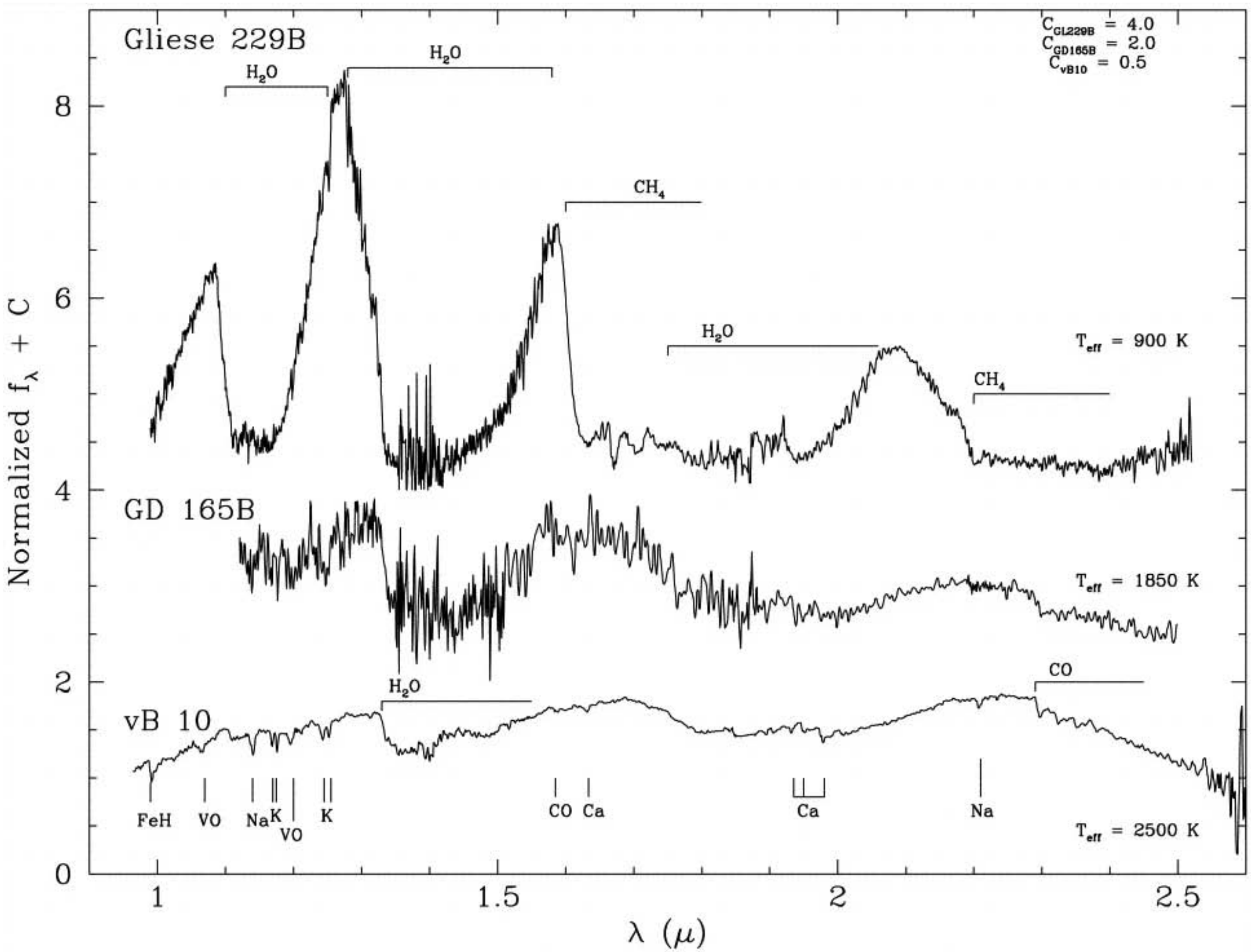

A giant planet candidate near a young brown dwarf★

Direct VLT/NACO observations using IR wavefront sensing

G. Chauvin[1], A.-M. Lagrange[2], C. Dumas[1], B. Zuckerman[3], D. Mouillet[4], I. Song[3], J.-L. Beuzit[2], and P. Lowrance[5]

A&A 425, L29–L32 (2004)

Another brown dwarf detected with the NACO adaptive optics system on the VLT

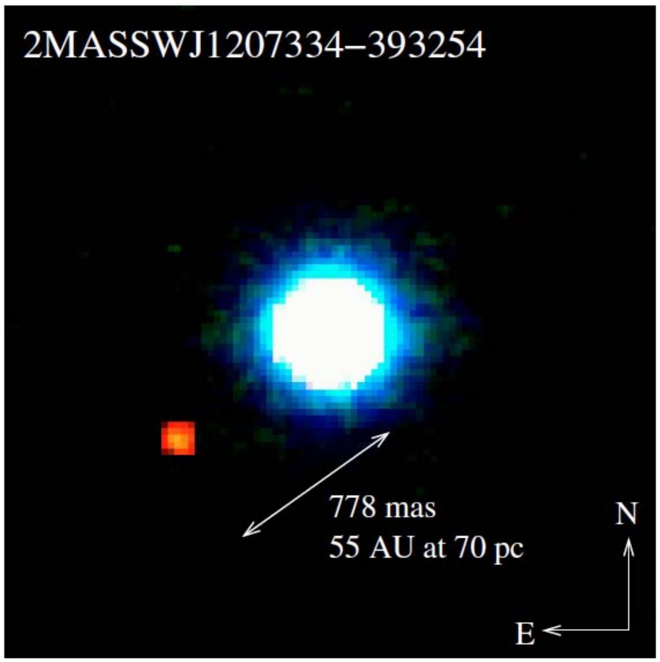

Fig. 1. Composite image of brown dwarf 2M1207 and its GPCC in *H* (*blue*), K_s (*green*) and *L′* (*red*). The companion appears clearly distinguishable in comparison to the color of the brown dwarf 2M1207.

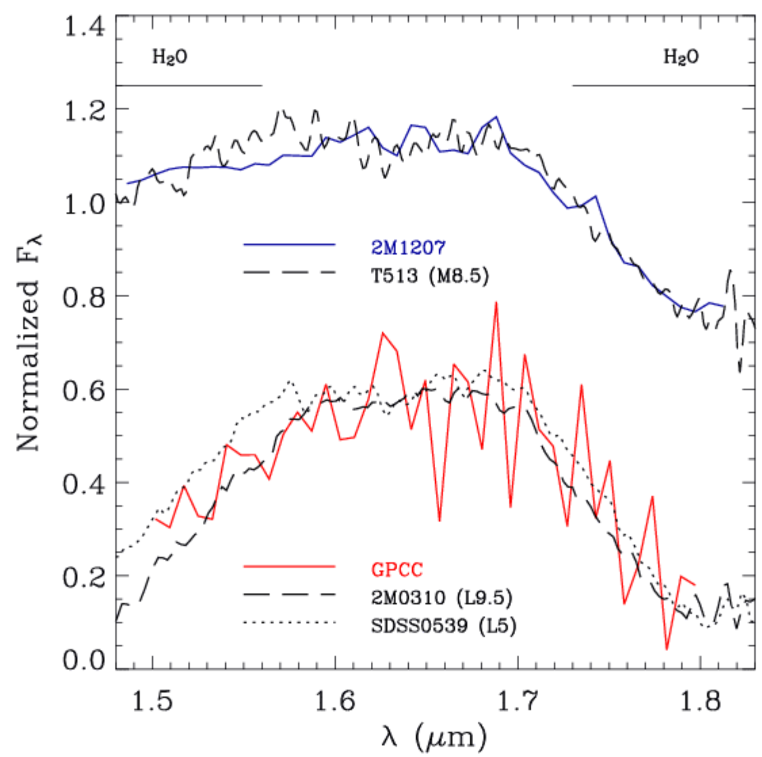

The Planet Candidate around GQ Lupi

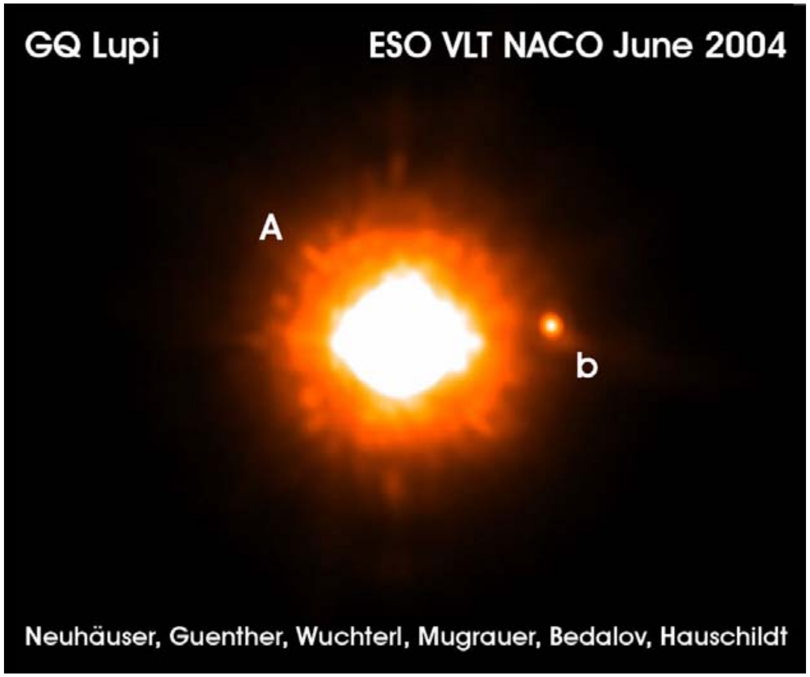

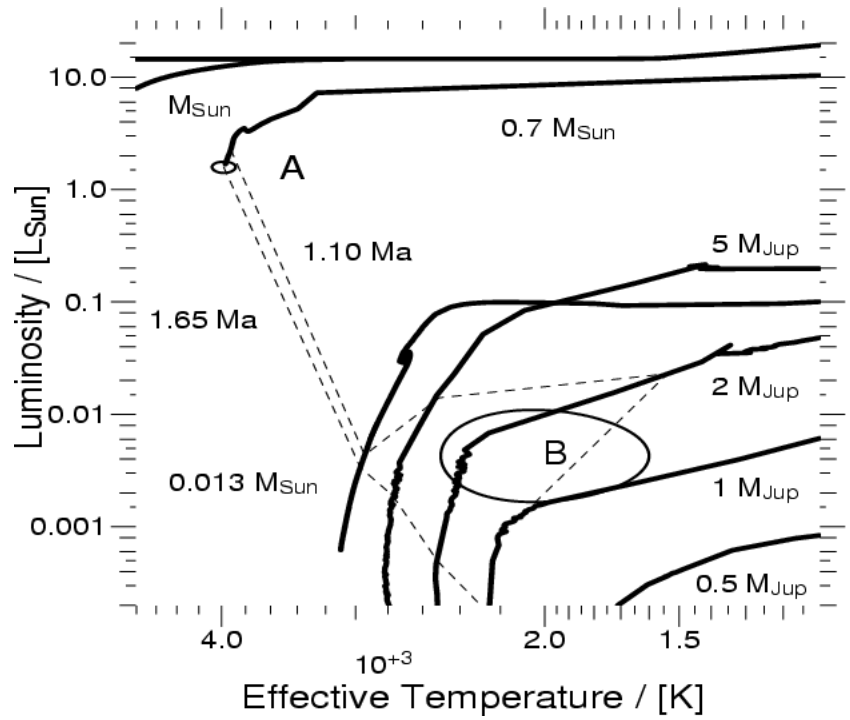

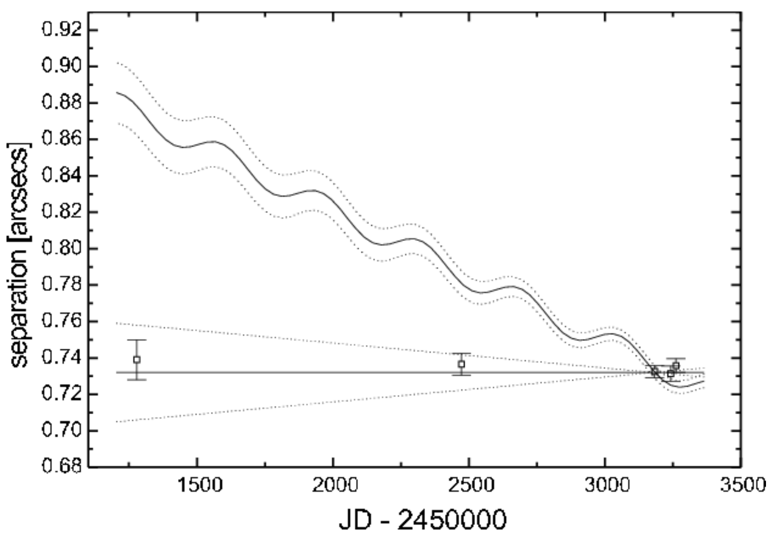

But there is large uncertainty in the surface gravity and mass can be as low as 4 and as high as 155 M_{Jup} **depending on which evolutionary models are used**.

A companion to AB Pic at the planet/brown dwarf boundary★

G. Chauvin[1], A.-M. Lagrange[2], B. Zuckerman[3], C. Dumas[1], D. Mouillet[4], I. Song[3], J.-L. Beuzit[2], P. Lowrance[5], and M. S. Bessell[6]

A&A 438, L29–L32 (2005)

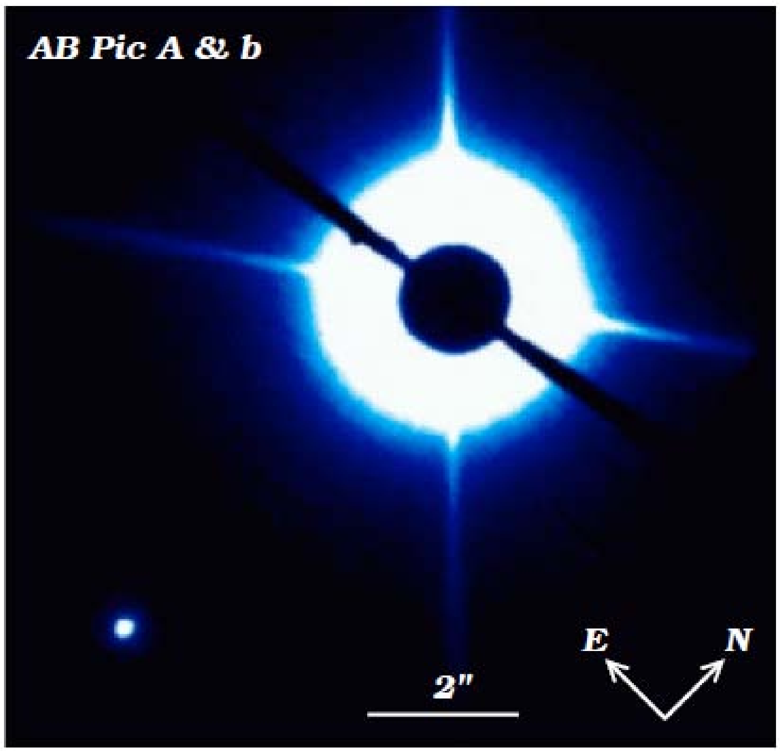

Fig. 1. K_s-band coronagraphic image of AB Pic A and b acquired on 17 March 2003 with an occulting mask of diameter 1.4″.

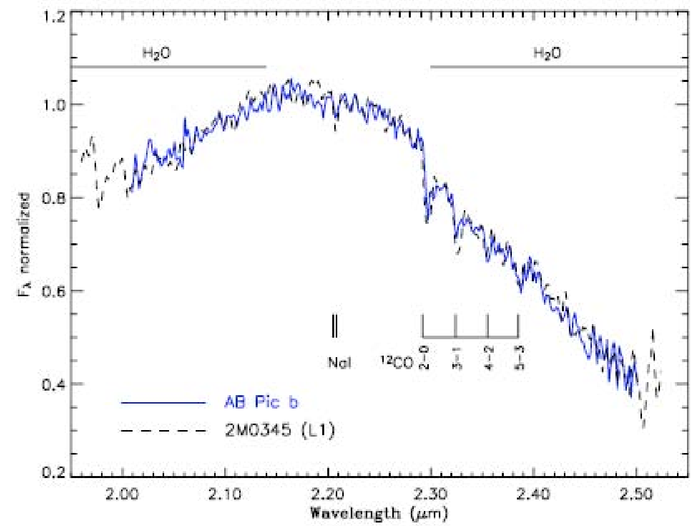

Fig. 3. K-band spectrum of AB Pic b acquired on 3 December 2004 with the low resolution ($R_\lambda = 550$) grism of NACO, the 86 mas slit and the S54 camera (54 mas/pixel). The best χ^2 adjustment is found with the L1 dwarf 2MASSJ0345+2540 (Geballe et al. 2002).

Estimated mass from evolutionary tracks: 13-14 M_{Jup}

Coronographic observations with HST

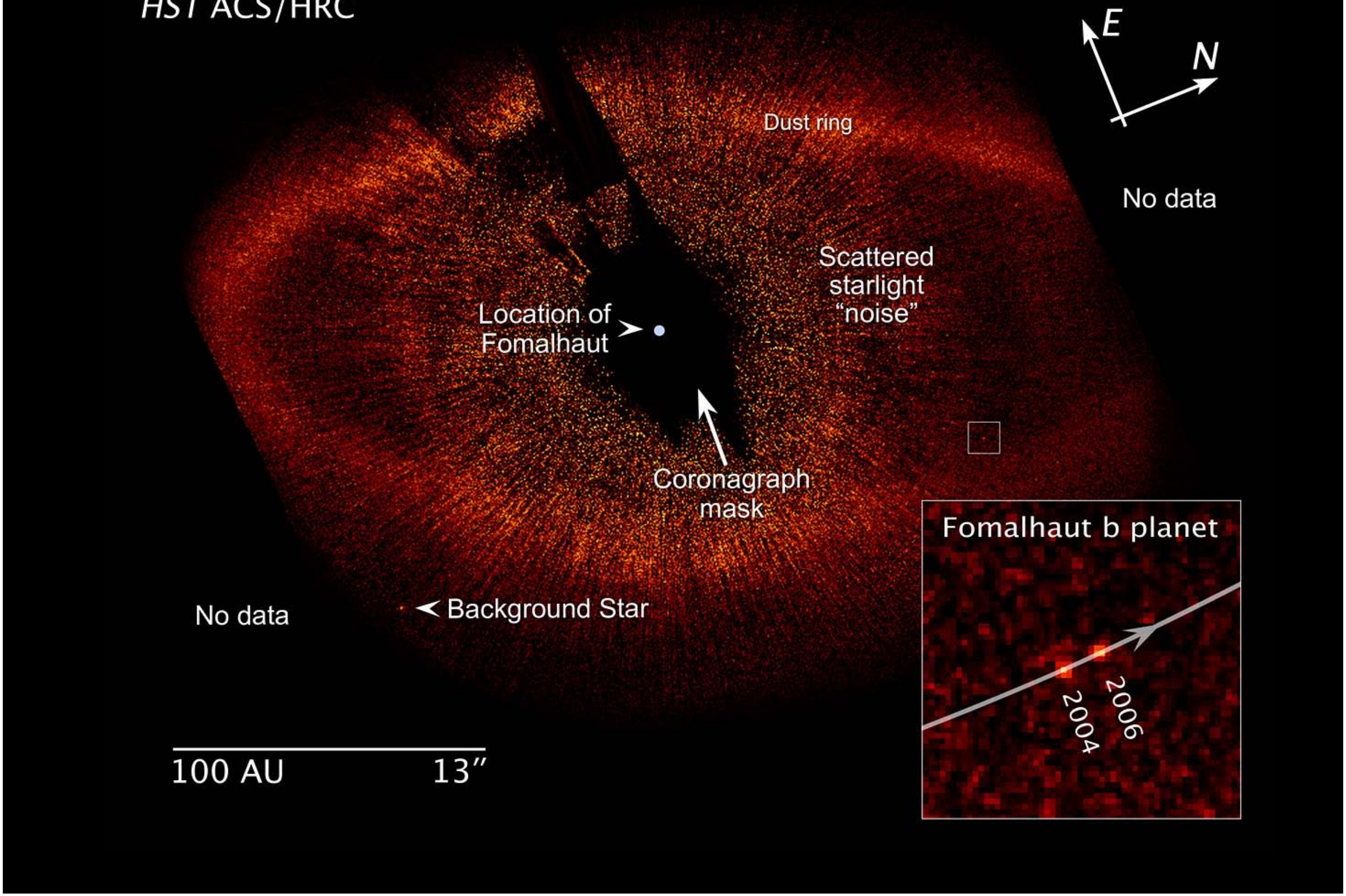

Optical Images of an Exosolar Planet 25 Light Years from Earth*

Paul Kalas[1*], James R. Graham[1], Eugene Chiang[1,2], Michael P. Fitzgerald[3], Mark Clampin[4], Edwin S. Kite[2], Karl Stapelfeldt[5], Christian Marois[6], John Krist[5]

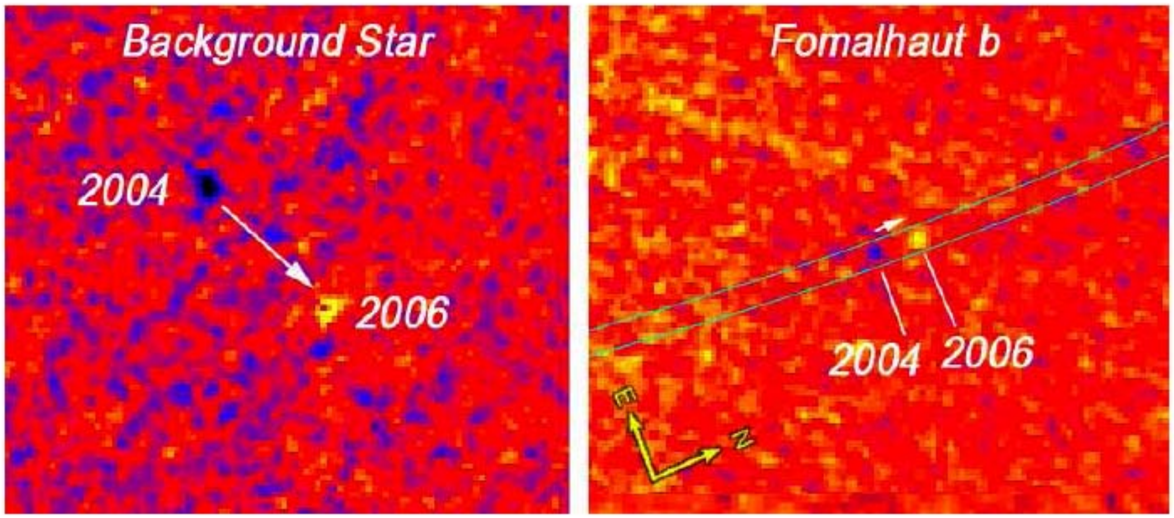

a ~ 115 AU

P ~ 870 years

Mass < 3 M_{Jup}, any more and the gravitation of the planet would disrupt the dust ring

Figure 4: **Fig. S1**: Two enlarged sub-regions (at the same scale) from Figure 1 centered on Fomalhaut b and a background star (located at the 8 o'clock position relative to Fomalhaut in Fig. 1, just outside the dust belt). We show relative motion by registering the 2004 and 2006 data to Fomalhaut and producing the difference image. Background objects are easily distinguished from the planet candidate in terms of the magnitude (0.7 arcsecond) and direction of their motion. In 2004, Fomalhaut b is detected at separation $\rho = 12.61''$ and position angle, PA = 316.86° relative to Fomalhaut. In 2006, Fomalhaut b is at $\rho = 12.72''$ and position angle, PA = 317.49° (recall that the orientation shown here is rotated 66.0° clockwise from one that gives north up and east left).

Photometry of Fomalhaut b

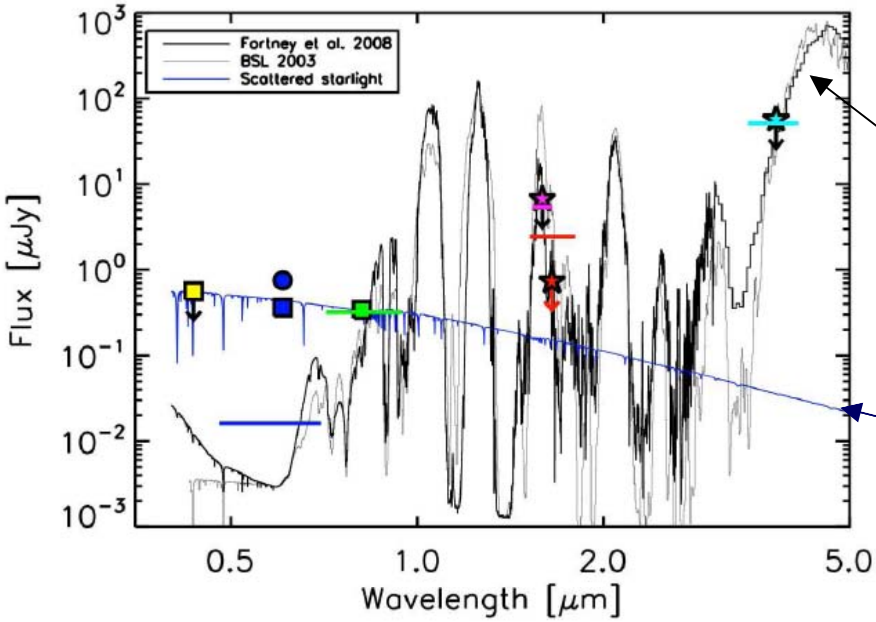

Planet model with T = 400 K and R = 1.2 R_{Jup}.

Reflected light from circumplanetary disk with R = 20 R_{Jup}

Figure 3: Photometry on Fomalhaut b shows the F435W 3-σ upper limit (yellow square), two F606W measurements (blue square=2006, blue circle=2004), the F814W photometry (green square), 3-σ upper limits for Keck observations in the CH_4 passband (purple solid star) and the H band (red solid star), and a 3-σ upper limits for Gemini observations at L' (light blue star). This is a log-log plot. If we first assume that the F606W variability is due to Hα emission and the F814W detection is due to planet thermal emission, we then proceed to fit a planet atmosphere model from (*15*) to the F814W flux. The heavy solid line represents that planet atmosphere model smoothed to R=1200 with planet radius 1.2 R_J, gravity 46 m s^{-2}, and T=400K (roughly 1-3 M_J at 200 Myr). The horizontal colored lines mark the equivalent broad-band flux found by integrating the model spectrum over the instrumental passband. Other models from (*16*) give a similar spectrum (light solid line), though a factor of 3 - 4 brighter in CH_4 and H band. The model predicts that the planet candidate should have been detected with Keck in the H band, though this prediction is only a factor of a few above our limit. The discrepancy could arise from uncertainties in the model atmosphere (which has never been tested against observation), or from the possibility that the F606W and F814W detections include stellar light reflected from a circumplanetary dust disk or ring system. The solid blue line intersecting the optical data represents light reflected from a circumplanetary disk with radius 20 R_J, a constant albedo of 0.4, and with stellar properties adopted from (*22*).

Detection of the planet in the optical may be due to a disk around the planet. Possible since the star is only 30 Million years old.

Direct Imaging of Multiple Planets Orbiting the Star HR 8799

Christian Marois,[1,2,3*] , Bruce Macintosh,[2] Travis Barman,[4]
B. Zuckerman,[5] Inseok Song,[6] Jennifer Patience,[7]

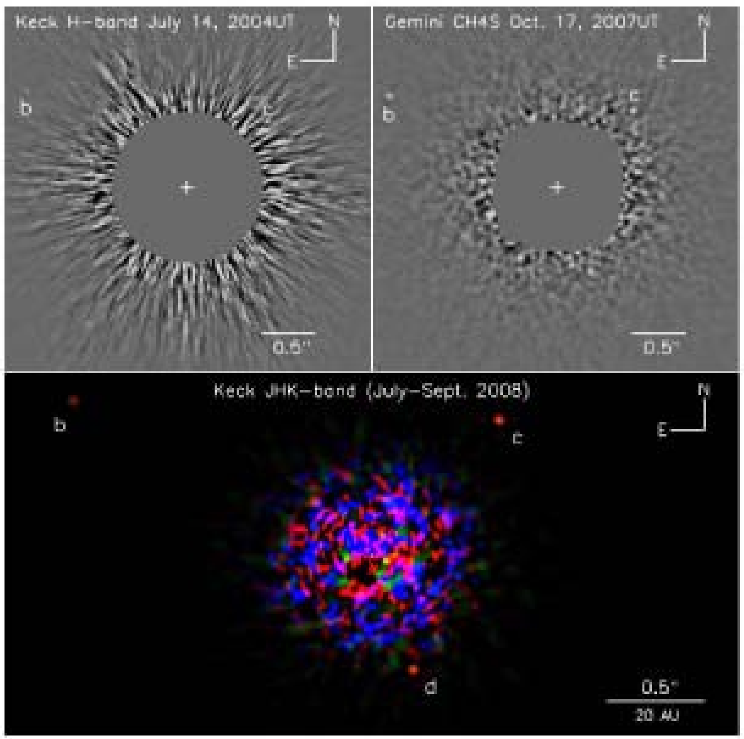

Figure 1: HR 8799bcd discovery images after the light from the bright host star has been removed by ADI processing. (Upper left) A Keck image acquired in July 2004. (Upper right) Gemini discovery ADI image acquired in October 2007. Both b and c are detected at the 2 epochs. (Bottom) A color image of the planetary system produced by combining the J-, H-, and Ks-band images obtained at the Keck telescope in July (H) and September (J and Ks) 2008. The inner part of the H-band image has been rotated by 1 degree to compensate for the orbital motion of the d between July and September. The central region is masked out in the upper images but left unmasked in the lower to clearly show the speckle noise level near d.

using

Angular Differential Imaging (ADI):

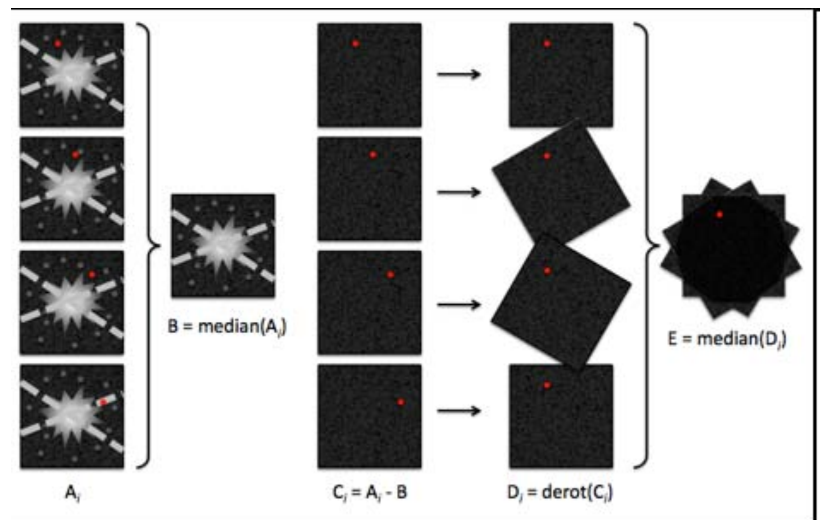

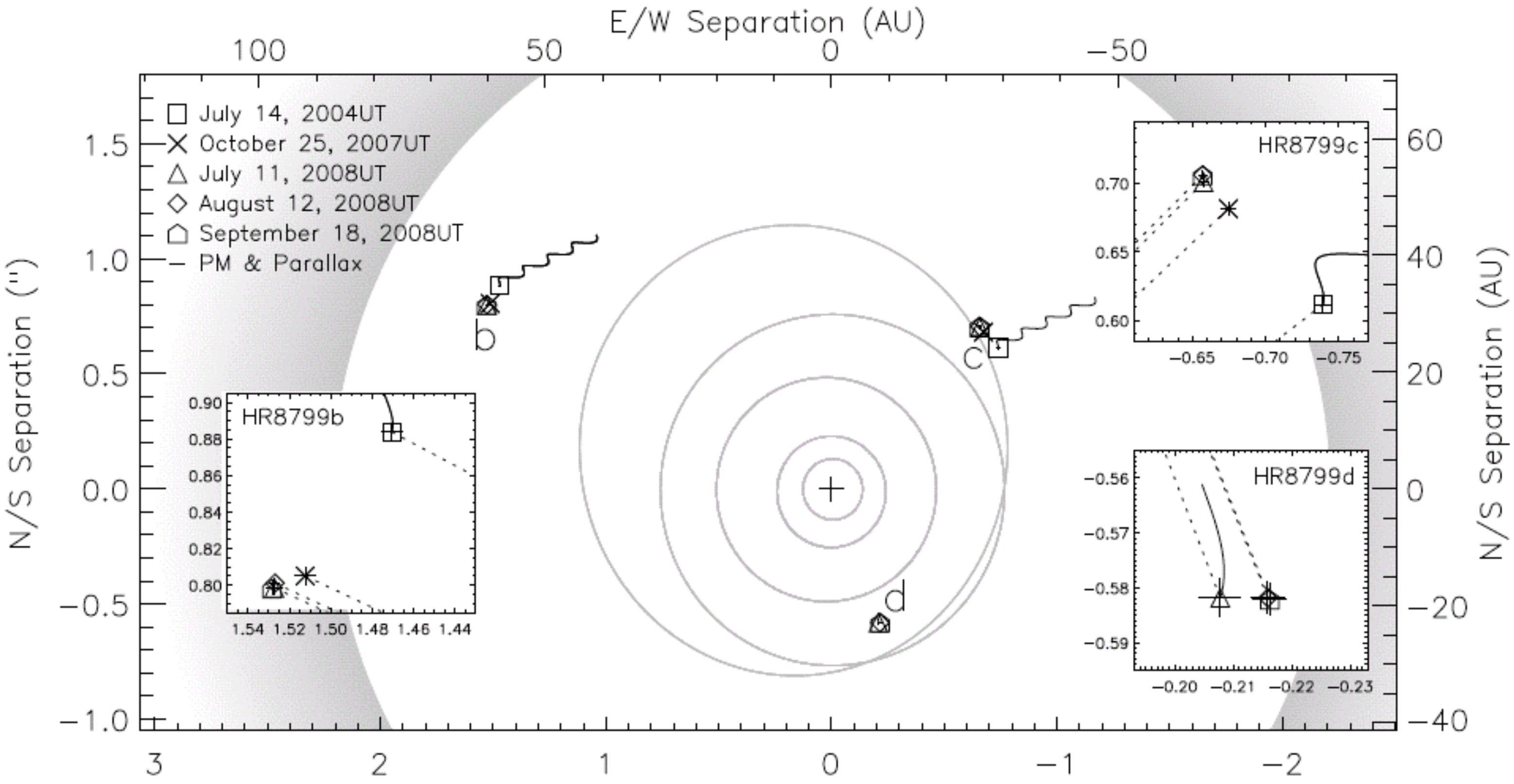

Figure 2: HR 8799bcd astrometric analysis. The positions of HR 8799bcd at each epoch are shown in both the overall field of view and in the zoomed-in insets. The solid oscillating line originating from the first detected epoch of each planet is the expected motion of a unbound background objects relative to the star over a duration equal to the maximum interval over which the companions were detected (4 years for b and c, two months for d.) All three companions are confirmed as co-moving with HR 8799 to 98σ for b, 90σ for c and $\sim$ 6σ for d. Counter-clockwise orbital motion is observed for all three companions. The dashed lines in the small insets connect the position of the planet at each epoch with the star. A schematic dust disk – at 87 AU separation to be in 3:2 resonance with b while also entirely consistent with the far-infrared dust spectrum – is also shown. The inner gray ellipses are the outer Jovian-mass planets of our Solar system (Jupiter, Saturn, Uranus & Neptune) and Pluto shown to scale.

The Planets of HR 8799 on Evolutionary Tracks

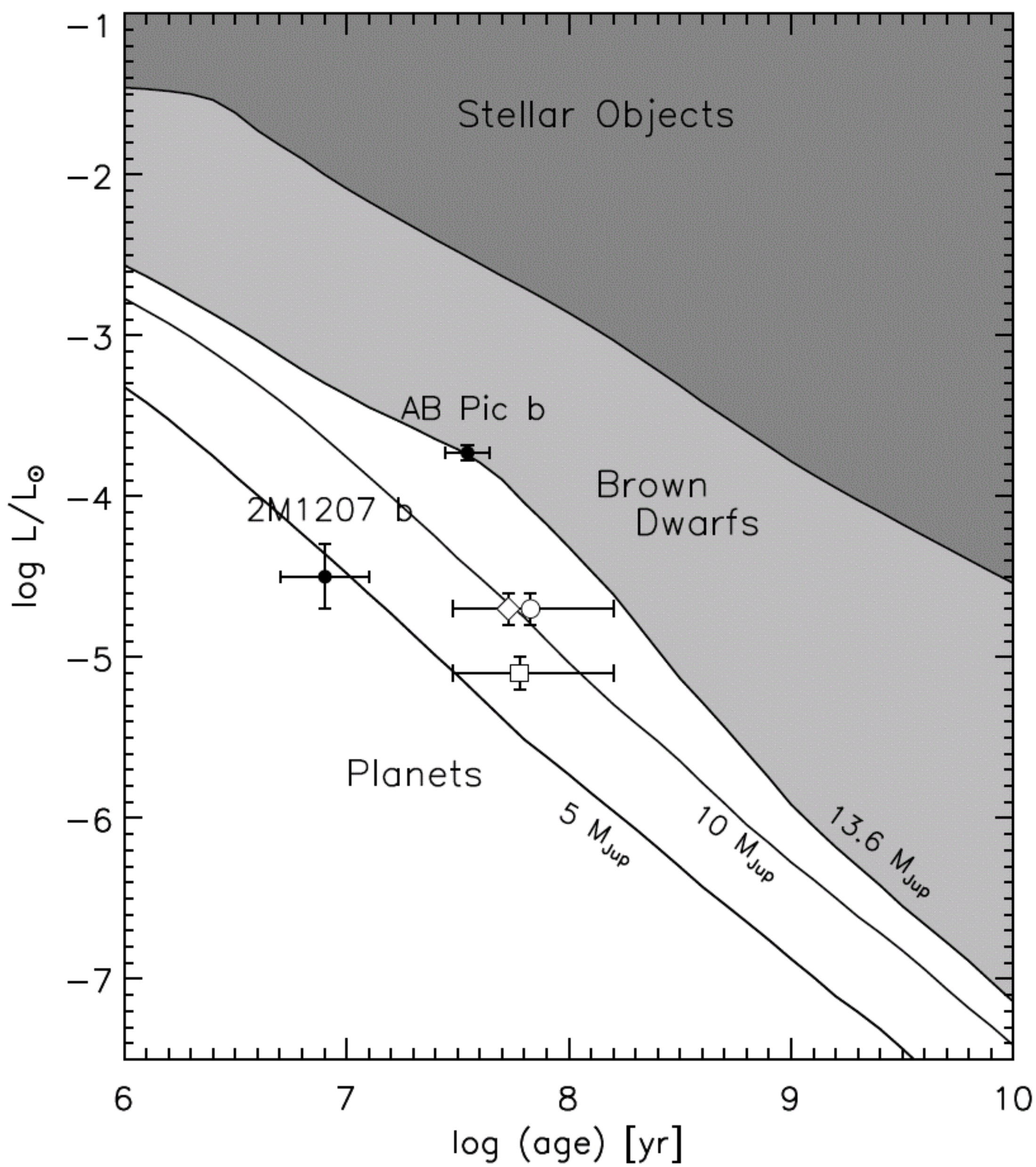

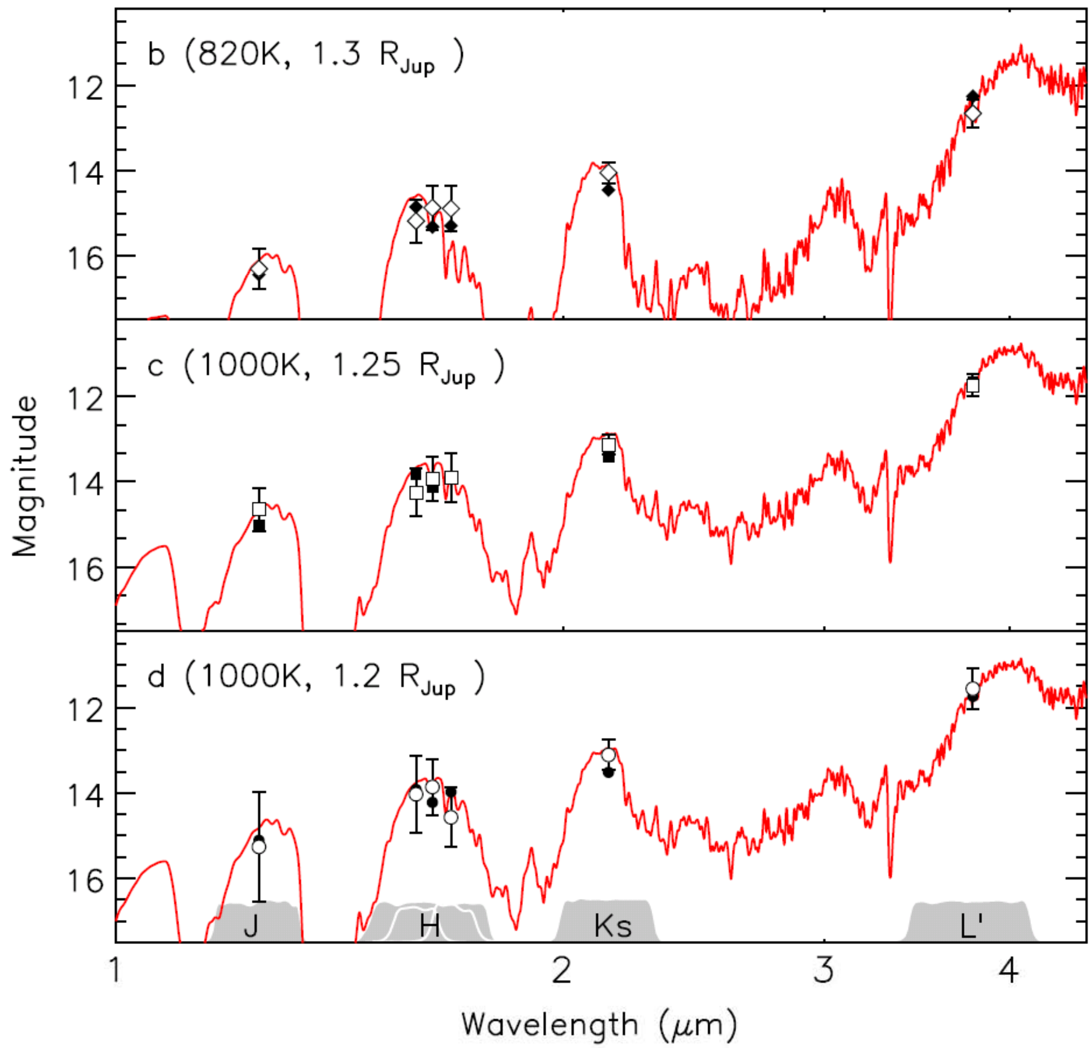

Figure 5: Synthetic spectra from model atmospheres containing clouds located between 10 and 0.1 bar of pressure are compared to the measured fluxes (with 3 sigma error bars) for HR 8799 b, c and d. Response curves for each filter band pass are indicated along the x-axis. The predicted magnitudes from the synthetic spectra, averaged over the filter passbands, are shown by the filled symbols.

The Planet around β Pic

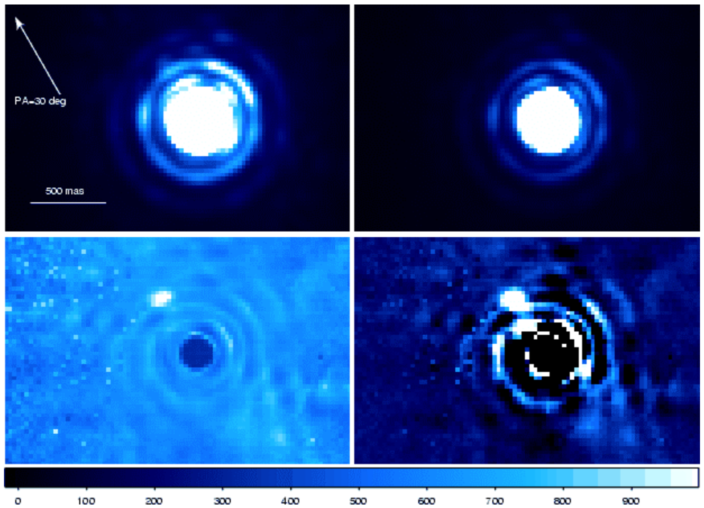

Mass ~ 8 M_{Jup}

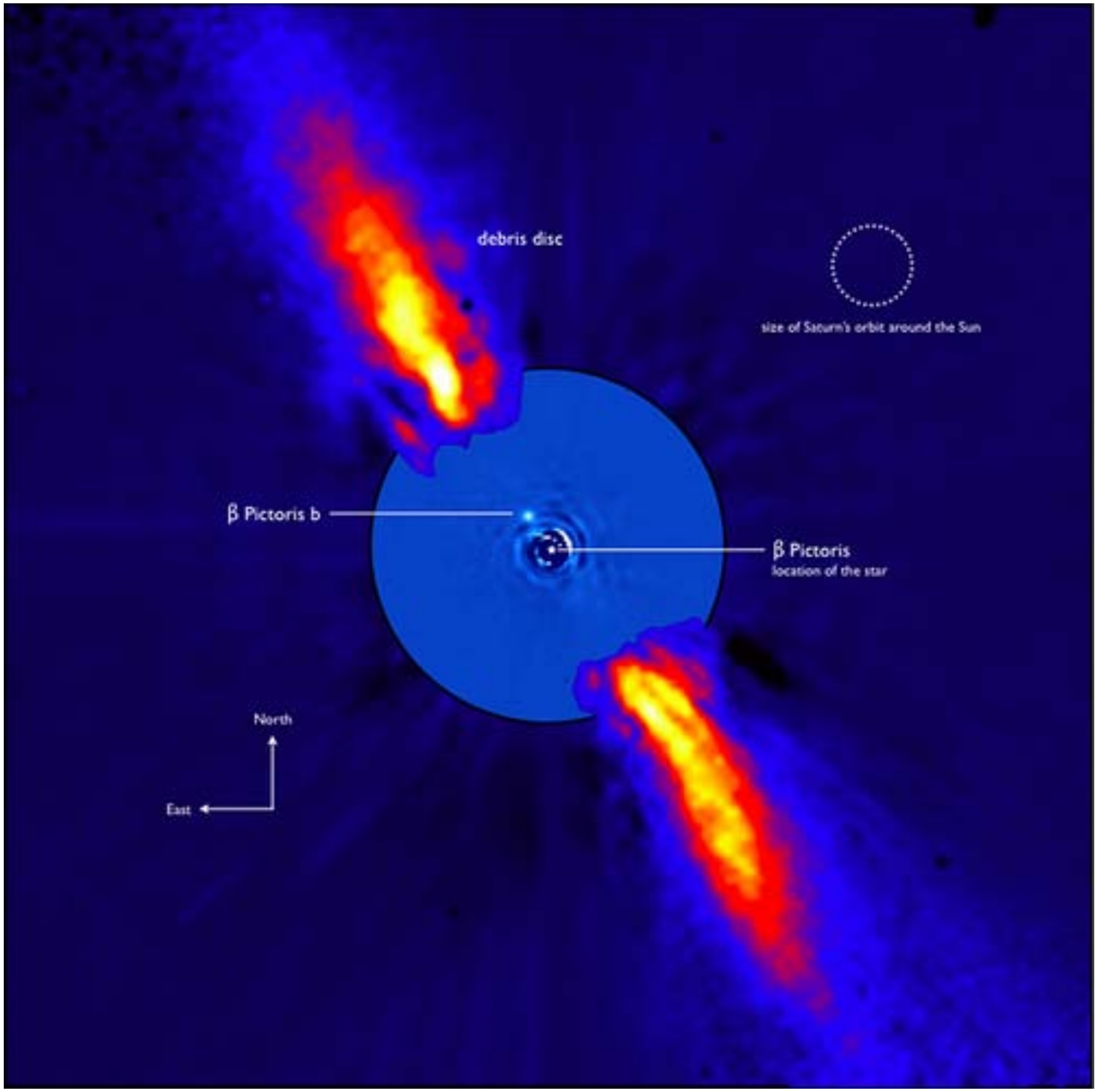

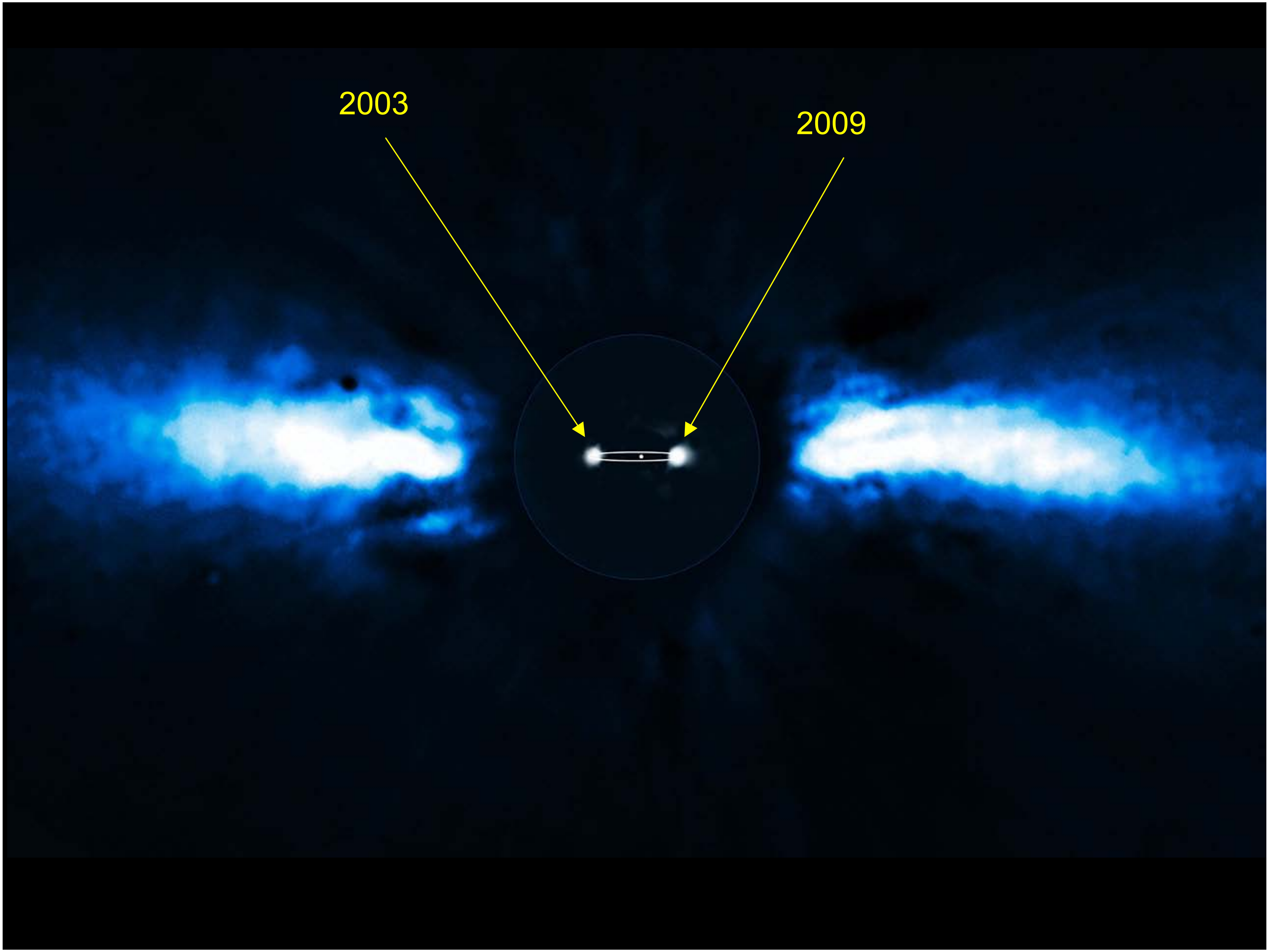
2003
2009

Imaging Planet Candidates

Planet	Mass (M_J)	Period (yrs)	a (AU)	e	Sp.T.	Mass Star
2M1207b	4	-	46	-	M8 V	0.025
AB Pic	13.5	-	275	-	K2 V	
GQ Lupi	4-21	-	103	-	K7 V	0.7
β Pic	8	12	~5	-	A6 V	1.8
HR 8799 b	10	465	68	-	F2 V[1]	
HR 8799 c	10	190	38	´-		
HR 8799 d[2]	7	10	24	-		
Fomalhaut b	< 3	88	115	-	A3 V	2.06

[1]SIMBAD lists this as an A5 V star, but it is a γ Dor variable which have spectral types F0-F2. Spectra confirm that it is F-type

[2]A fourth planet around HR 8799 was reported at the 2011 meeting of the American Astronomical Society

Summary of Direct Imaging:

- Most challenging observational technique due to proximity, contrast levels and atmospheric effects (AO, coronagraphy,..)
- Candidates appeared at large (~100 AU) separations and mass determination is limited by reliability of evolutionary models (if no other information)
- More robust detections (3) include a multi-planet system (HR 8799) and two planets around stars with a large debris disk (Fomalhaut, beta Pic)
- Massive planets around massive stars (A,F-type) at large separations (no Solar System analogues yet) *different class of exoplanets?*